Spontaneous differentiation across cell lineages of separate germ layer origin during progenitor cell-mediated regeneration of the central nervous system

Civia Z. Chen[1,2,3], Yizhou Yu[2,5], Natalia Murphy[2,4], Juan F. Cubillos[2,3], Khalil S. Rawji[1,2,3], Chao Zhao[1,2,3], Myfanwy Hill[2], Peter Arthur-Farraj[3,6], Robin J.M. Franklin[1,2,3], Björn Neumann[1,2,3]

[1]*Altos Labs Cambridge Institute, Granta Park, Cambridge UK*

[2]*Wellcome-MRC Cambridge Stem Cell Institute, University of Cambridge, UK*

[3]*Department of Clinical Neurosciences, University of Cambridge, UK*

[4]*Department of Veterinary Medicine, University of Cambridge, UK*

[5]*Department of Medicine, University of Cambridge, UK*

[6]*Blizard Institute, Queen Mary University of London, UK*

*Corresponding authors: Björn Neumann, bneumann@altoslabs.com;, Robin Franklin, rfranklin@altoslabs.com

SUMMARY

Under homeostatic conditions, axons of the central nervous system (CNS) are myelinated by oligodendrocytes. However, in response to demyelination, Schwann cells (SCs), the myelinating glia of the peripheral nervous system (PNS), can contribute to CNS remyelination. Lineage tracing studies demonstrated that many CNS remyelinating SCs, in addition to remyelinating oligodendrocytes, are derived from adult CNS stem cells called oligodendrocyte progenitor cells (OPCs). Here we describe the mechanisms by which the fate switch of neuroepithelial-derived OPCs into SCs, a cell normally of neural crest origin, occurs. Using single-cell RNA-sequencing we identified a subpopulation of OPCs within demyelinating lesions that co-express SC markers. Within this SC-primed group, differential gene analysis revealed a significant upregulation of genes involved in integrin signalling and bone morphogenetic protein (BMP) activation. We found that BMP4 and vitronectin, an extracellular matrix molecule and integrin ligand, are sufficient external cues to induce SC differentiation by OPCs by directly exerting effects on the transcription factors OLIG2 and SOX10, which are critical regulators of cell fate in oligodendroglial cells and SCs. We also show that OPCs can be directly programmed toward a SC fate by suppressing the expression levels of *Olig2* and while maintaining those of *Sox10*. OPC-derived SCs morphologically and transcriptionally resemble primary SCs and can myelinate CNS axons with peripheral type myelin. Our findings indicate that injury-related changes in the environment can destabilise oligodendroglial transcription factor networks, enabling alternative OPC fate choices during CNS remyelination.

INTRODUCTION

A key function of adult tissue-specific stem cells is to contribute to regeneration of the tissue in which they reside following injury in which some or all components of the tissue are lost. This occurs in many tissues by the activation of adult stem cells within the vicinity of the injury, their expansion and ultimately their differentiation into replacement cells. In vertebrate species, differentiation is restricted to the cell types of their parent tissue. This lineage restriction means that during differentiation they do not generate cells derived from a germ layer different from the origin of the tissue[1–3]. A remarkable exception to this rule is the regenerative process of remyelination that occurs following central nervous system (CNS) demyelination (the loss of myelin sheaths from around otherwise intact axons). This regenerative response is mediated by a widespread population of adult CNS stem cells called oligodendrocyte progenitor cells (OPCs). In response to demyelination, OPCs become activated, migrate, proliferate and differentiate into a new myelinating cell. In the majority of cases, OPCs give rise to oligodendrocytes, as expected. However, in certain situations, notably when there is concurrent loss of astrocytes, OPCs, a cell of neuroepithelial origin, will generate Schwann cells (SCs)[4], the myelinating cells of the peripheral nervous system and a cell of neural crest origin. CNS remyelination by SCs is seen in clinical disease, such as multiple sclerosis (MS)[5,6] and traumatic CNS injury[7,8], as well as in a range of experimental models that cause demyelination[9–12]. The neural crest is now regarded as the "fourth" germ layer[13], making the differentiation of the neuroepithelium-derived OPC into a cell of neural crest origin a unique cross-germ layer event during tissue regeneration in experimental models of remyelination and in human disease.

The prevalent hypothesis to explain the molecular mechanism governing SC fate transitions from OPCs proposes that OPCs exposed to higher levels of BMP signalling will acquire SC fate as long as this signal is not opposed by the presence or activity of astrocytes in the lesion environment[14,15]. However, BMP signalling alone is insufficient to induce this fate transition in pure cultures of isolated OPCs (devoid of astrocytes and BMP inhibitors) *in vitro*, indicating the involvement of additional factors. Recently, Wnt[16] and NRG1/ErbB signalling[16,17] have been proposed. However, while both factors are required for OPCs to form SCs after transplantation into peripheral nerve lesions[18], the natural domain of PNS SCs, there is no evidence that these pathways play an instructive role in the process.

Identifying the elusive factors and understanding the mechanisms by which OPCs give rise to SCs is not only of intrinsic interest from the perspective of regeneration biology, given the uniqueness of its germ layer crossing properties, but may also have translational relevance. For example, therapeutically favouring SC remyelination could be reparative for multiple sclerosis (MS), as SC remyelinated axons could be inherently resistant to autoimmune attacks targeting CNS myelin.

Here, we identify both the extrinsic and intrinsic mechanisms that govern the spontaneous fate switching of endogenous adult OPCs into SC during remyelination and uncover key transcription factors capable of diverting OPCs into a SC fate *in vitro* and *in vivo*. This work provides a foundation for exploring the evolutionary origins of myelin and has broad implications for regenerative medicine and cellular reprogramming.

RESULTS

Transcriptomic profiling of OPCs activated by demyelination reveals a Schwann cell-primed subpopulation

Within an area of demyelination undergoing remyelination by both oligodendrocytes and SCs there will be distinct populations of OPC destined to become either one of the two remyelinating cell types, as well as a population that will remain as OPCs to re-establish their pre-lesion density[4]. We reasoned that if we could capture these distinct populations within a lesion undergoing remyelination using a single cell sequencing strategy, we could identify key pathways involved in achieving specific cell fates, including differentiation into a remyelinating SC. To do this and thereby characterise the transcriptomic landscape of OPCs at the onset of differentiation, we used a well-established *in vivo* model of demyelination/remyelination in which ethidium bromide is injected into the caudal cerebellar peduncle of adult rats[12]. Using this model, lesions were dissected at 10 days after lesion induction, at which time OPCs recruited into the lesion are beginning to undergo differentiation[19], and the tissue subjected to Smartseq2 single cell transcriptomics. This yielded 517 high-quality cells across three biological replicates (Figure 1A, Supplementary Figure 1 A, B).

Unsupervised clustering identified five distinct clusters (Figure 1B). We identified a SC-primed cluster that showed expression of SC markers (*Pou3f1, Mpz, Egr2, Prx, Pmp22*) in addition to OPC markers. This cluster was significantly enriched in the lesion compared to uninjured tissue (Supplementary Figure 1C) and expresses high levels of SC-related genes (Supplementary Figure 1D). The remaining clusters included an oligodendrocyte (OL) primed cluster that highly expresses OL markers (*Plp1, Opalin, Myrf, Mbp*), a progenitor cluster enriched in OPC markers (*Pdgfra, Cspg4, Ascl1*), an OPC transition cluster, which expressed a hybrid selection of genes across the oligodendroglial lineage, and a cluster that was more enriched in genes related to astrocytes (*Gfap*, *Aqp4*, *Sox9*, *Aldh1l1*) (Supplementary Figure 1E). These findings reveal a subset of injury-responsive OPCs capable of upregulating SC-specific transcripts, suggesting they likely contribute to SC differentiation in the lesion environment *in vivo*.

To examine whether the cluster of OPCs expressing SC markers contained the cells destined to become remyelinating SCs, we performed trajectory analysis using graph abstraction[20]. We observed that SC-

primed cells had higher pseudotime values than progenitor cells, suggesting that SC-primed cells represent a more advanced or committed state in the differentiation trajectory (Figure 1D and Supplementary Figure 1F). To further investigate OPC-to-SC differentiation and identify potential signalling pathways by which it might occur, we used CellRank2 to model cell-to-cell transitions using diffusion pseudotime. We then quantified fate commitment by estimating each cell's absorption probability towards the SC state[21]. This analysis showed that OPCs in the SC-primed cluster have the highest probability of committing to a SC fate (Figure 1E). These results, along with our trajectory analysis, strongly suggest that the SC-primed cluster represents a population of OPCs with a distinct lineage commitment toward a SC fate.

Correlating these fate probabilities with gene expression allowed us to pinpoint the molecular programs driving this fate decision. This revealed that commitment to a SC lineage was significantly associated with the upregulation of pathways related to extracellular matrix (ECM) organization and integrin signalling, as well as SC differentiation (Figure 1F). Key driver genes systematically upregulated along this trajectory included *Egr2* and *Sox10* (Figure 1G)**.** We also identified the Wnt pathway previously implicated in the induction of SC differentiation by OPCs[16,22] Supplementary 1G).

Vitronectin and BMP4 are sufficient to drive OPC to SC differentiation

In tissue culture, BMPs induce OPC differentiation into astrocytes and not SCs[23]. This suggests that within a lesion environment, other signals in addition to BMPs are required to generate SCs. The analysis of the SC-primed cells identified ECM-integrin engagement as a prime candidate for the additional co-factor. Several ECM genes have increased expression during the remyelination that follows toxin-induced experimental demyelination, including laminin α2, tenascinC/R, osteopontin, vitronectin and fibronectin[24]. We focused our initial studies on vitronectin, which is closely related to fibronectin and fulfilled criteria we deemed critical for the elusive factor. Vitronectin is highly abundant in the lesion area during remyelination and can be bound by OPCs via αV integrin[24–27]. Further, it is mainly plasma derived and therefore present from early timepoints after lesion induction that causes the blood brain barrier to become leaky. Blood plasma as the source of vitronectin also offered a possible explanation why SC remyelination occurs often in close proximity to the blood vessels[16]. Moreover, it has been shown to

coordinate with and potentiate BMP signalling[28]. By contrast, laminin α2 is expressed in lesion models after the appearance of SCs[24], while tenascins are largely expressed by astrocytes[29] and therefore unlikely to be involved in SC differentiation given that astrocytes are associated with the suppression of SC differentiation from OPCs. We excluded osteopontin because we had previously shown that there is no change in SC remyelination in osteopontin deficient mice[30]. We therefore hypothesised that co-treatment with BMP4 and vitronectin might recapitulate the key signals present in the *in vivo* environment responsible for directing OPCs toward a SC fate[31–33] (Figure 2A). OPCs grown under these conditions acquired a spindle-like morphology with elongated nuclei, which, upon confluency, formed a wavelike pattern similar to that of cultured primary SCs. These cells were immunoreactive to S100b, GFAP, and SOX10 with the same intensity and sub-cellular localisation to that of primary SCs (Figure 2B). In contrast, adult OPCs grown under standard conditions on PDL-coated plates retained a round morphology and high expression of OLIG2 and SOX10 (Figure 2C).

To determine whether this switch to a SC fate required the combination of these two factors, vitronectin and BMP4, we next examined the effect of each factor individually. Consistent with prior reports[23,34], we observed that treatment with BMP4 alone promoted OPC differentiation into GFAP$^+$ astrocytes. (Supplementary Figure 2A). We then tested the effect of vitronectin alone to distinguish whether it acts as a permissive co-factor or as an instructive signal. First, we assessed its impact on progenitor maintenance. When cultured under proliferation conditions (with the growth factors PDGF and FGF), vitronectin had no effect on the number of A2B5$^+$/NG2$^+$ OPCs compared to PDL controls, indicating it does not affect OPC survival or proliferation (Supplementary Figure 2B, C). Next, we determined if vitronectin altered the differentiation potential of OPCs into oligodendrocytes using an established differentiation cue, thyroid hormone (T3)[35]. Following 5 days of T3 treatment, OPCs cultured on vitronectin differentiated into MBP-positive oligodendrocytes, however there was a reduction in MBP$^+$ cells compared to the PDL control (Supplementary Figure 2D). These results demonstrate that while vitronectin does not independently alter oligodendroglial identity, it likely acts as a permissive co-factor, redirecting the outcome of BMP4 signalling away from astrocyte generation and towards a SC fate.

To map the transcriptional programs driving the early stages of OPC-to-SC differentiation, we performed single-cell RNA sequencing using 10x Genomics on OPCs three days after treatment with vitronectin and

BMP4. Unsupervised clustering resolved five cellular states referred to as B0 to B4 (Figure 2D). Subsequent RNA velocity pseudotime to elucidate how these distinct clusters related to one another[36] revealed a single, continuous differentiation trajectory that originated from a progenitor-like state that co-expressed initial SC genes (B1; *Pdgfra, Itga1, Dag1, Src)*, progressed through intermediate populations expressing SC genes such as *Pmp22* (B0, B4), and culminated in a single, terminal cluster (B3) that was most advanced in pseudotime (Figure 2E). The direction of this trajectory was strongly correlated with the highest expression of SC markers (*Pou3f1, Src, Erbb3, Ntrk2, Itga1*) (Figure 2F, Supplementary 3A).

To understand the molecular identity of the emerging OPC-derived SC (oSC) population, we focused our analysis on the most mature SC-like cluster (B3) from our single-cell dataset. Gene expression analysis revealed a hybrid transcriptional profile in that they contained genes associated with both OPCs and SCs. When compared to the progenitor clusters (B0/B1), cluster B3 was, as expected, highly enriched for SC-related genes (*Pou3f1, Sox10, Pmp22, Erbb3*). However, we also observed a significant upregulation of genes and transcription factors associated with CNS myelination and early oligodendrocyte progression (*Olig1, Myrf, Opalin, Mag, Mbp*) (Supplementary 3B, C). This was supported by the co-expression of both SOX10 and low levels of OLIG2 within the B3 population (Supplementary Figure 3D), suggesting that these newly induced oSCs represent an immature, transitional state still retaining features of their oligodendroglial origin**.**

This finding led us to hypothesise that, like primary SCs, these immature oSCs would require additional extrinsic cues to complete their maturation into a myelinating cell. To test this, we cultured the newly induced oSCs in a standard SC differentiation medium containing neuregulin and cAMP[37]. We then used RT-qPCR to compare newly induced oSCs to differentiated oSCs, primary SCs and primary OPCs. Newly induced oSCs expressed markers of immature SCs (*p75, S100b)* at levels comparable to primary SCs, but their expression of genes associated with a myelinating phenotype (*Pou3f1*, *Egr2*) was lower (Figure 2G). In contrast, differentiated oSCs were transcriptionally indistinguishable from primary SCs across all markers tested (Figure 2G). These findings demonstrate that vitronectin and BMP4 treatment initiates a switch to an immature SC fate, and that these oSCs are fully competent to respond to developmental cues, suggesting the potential to achieve a mature, peripheral, myelinating phenotype.

Extrinsic factor-induced oSCs are able to myelinate CNS axons *in vivo*

Having established that adult OPCs can be induced to differentiate into SCs *in vitro* by exposure to a combination of vitronectin and BMP, we next asked whether SCs so generated could form myelin sheaths around CNS axons. To test this, we induced OPC-to-SC differentiation by culturing OPCs on vitronectin with BMP4, expanded the cells in standard growth medium, and labelled them by transfection with a lentiviral vector containing the mCherry fluorescent reporter gene. Using the same model of CNS demyelination-remyelination that was earlier used to capture single-cell sequencing data of OPCs at the onset of the differentiation phase of remyelination, mCherry-labelled oSCs were transplanted unilaterally into the caudal cerebellar peduncle (CCP) one week after inducing bilateral ethidium bromide (EB)-mediated demyelinating lesions (Figure 3A). The lesioned area was assessed three weeks post-transplant (28 days post-lesion). Since SC remyelination is a feature of spontaneous repair in EB-CCP lesions[38], we expected the total SC remyelination would involve contributions from both endogenous and transplanted SCs. Therefore, we quantified total SC remyelination by counting cells that expressed periaxin (PRX), a protein specific to myelinating SCs but not oligodendrocytes. We identified those that were of transplant origin by the co-expression of mCherry and PRX. In the transplanted (left) hemisphere there were 2415 ± 1029 PRX^+ cells / mm^2, of which 682 ± 169 cells / mm^2 were also $mCherry^+$ (Figure 3B, C). No $mCherry^+$ cells were detected in the non-transplanted contralateral lesions, which served as an internal control. The total amount of endogenous SC remyelination (quantified by the number of $mCherry^-PRX^+$ cells) in these control lesions was similar to that on the transplanted side, suggesting that transplanted SCs did not enhance differentiation of endogenous OPCs into SCs (Figure 3C, D). Furthermore, transplantation did not affect overall lesion pathology, as there were no significant differences in lesion size, quantified by the area with a loss in fluorescence intensity following immunohistochemistry of tissue containing lesions with antibodies against the major myelin protein, MBP. There was also no significant difference in the microglia recruitment or astrocytic hypertrophy between the left and right CCP, denoted by immunoreactivity to IBA1 and GFAP respectively (Figure 3E, F).

Injury-associated ECM signalling induces decreased expression of Olig2 but sustains levels of Sox10 in OPCs transitioning towards SCs

Having established niche-associated factors that will induce the differentiation of oSCs, we next asked by what internal mechanisms this process occurs with specific reference to the transcription factors involved

as these are key regulators of cellular identity, guiding lineage commitment and differentiation. The transcription factors SOX10 and OLIG2 are central to glial identity, and within the oligodendrocyte lineage, they form a positive feedback loop to stabilise lineage commitment[39,40]. While SOX10 is also a master regulator for SC development[41], OLIG2 is considered a specific and essential pioneer factor for oligodendrocytes[42,43]. Based on this, we hypothesised that the OPC-to-SC differentiation requires the loss of OLIG2 to permit a SOX10-driven SC transcriptional program. To test this, we first re-examined our *in vivo* Smart-seq2 dataset from the demyelinated CCP. This analysis confirmed that the SC-primed OPC cluster expressed high levels of *Sox10*, but significantly lower levels of *Olig2* compared to the oligodendrocyte-primed cluster (Figure 4A).

To experimentally validate the SOX10/OLIG2 switch in OPCs required for SC differentiation predicted by our hypothesis and bioinformatic analyses, we tested the effects of vitronectin and BMP4 alone and in combination on the expression of these two genes. We predicted that induction of oSCs by the combination of vitronectin and BMP4 would result in a commensurate decrease in *Olig2* expression, while maintaining *Sox10* levels. RT-qPCR revealed that OPCs cultured on vitronectin exhibited a significant reduction in *Olig2* transcript levels compared to cells grown on PDL under standard conditions (Figure 4B). This effect was amplified by the addition of BMP4 (Figure 4C). Consistent with these findings, OLIG2 protein expression, visualised by immunohistochemistry, was similarly decreased (Figure 4D, E).

In contrast, while *Sox10* transcript levels decreased in OPCs cultured on vitronectin and were further reduced upon BMP4 treatment **(**Figure 4B, C), this transcriptional reduction was not reflected at the protein level. Quantification of fluorescence intensity showed that SOX10 protein was robustly maintained in the nucleus in cells cultured on vitronectin and treated with BMP4, but not for cells cultured on PDL (Figure 4D), highlighting a potential post-transcriptional mechanism that preserves SOX10 expression. To test the hypothesis of enhanced protein stability directly, we performed a cycloheximide (CHX) chase assay. Western blot analysis following the CHX block revealed that the half-life of the SOX10 protein was extended in cells treated with vitronectin and BMP4 compared to controls (Figure 4F). Together, these findings suggest that injury-associated ECM signalling drives OPC-to-SC differentiation by downregulating *Olig2* and *Sox10* to suppress an oligodendrocyte differentiation programme, while simultaneously sustaining SOX10 protein levels required to promote SC differentiation.

Olig2 knock down and Sox10 overexpression can induce OPC-to-SC differentiation

We next addressed whether direct genetic manipulation of *Olig2* and *Sox10* could phenocopy the effects of the extrinsic signals, vitronectin and BMP4. For this, we first generated and validated lentiviral constructs to overexpress *Sox10* or to knock down *Olig2* levels using an *Olig2* shRNA lentivirus (Supplementary Figure 4A). We confirmed successful overexpression and knockdown using qPCR, western blot and immunofluorescence (Supplementary Figure 4B-E).

We first used these viral vector tools to determine if OLIG2 suppression is the primary downstream event of the BMP4 signal. We reasoned that if this were so, then in a system where SOX10 is overexpressed, the pro-SC gene expression programme should be activated regardless of whether OLIG2 is suppressed chemically (by BMP4) or genetically (by shOlig2). Indeed, we observed no significant difference in a panel of key SC marker genes (*Olig2*, *Sox10*, *Pdgfra*, *Myrf*, *Gfap*, *p75*, *S100b*, *Pou3f1*, *Krox20*) between cells treated with SOX10 and shOlig2, or SOX10 and BMP4 (Supplementary Figure 4F). Having established that BMP4 contributes to the SC fate switch by reducing OLIG2 levels, we next asked if we could phenocopy the effects of vitronectin and BMP4 by simultaneously overexpressing *Sox10* and knocking down *Olig2* (hereafter referred to as 'TF-induced') (Figure 5A). Indeed, in contrast to the rounded, branched morphology of uninfected OPCs, OPCs co-infected with both lentiviruses underwent a profound phenotypic conversion, acquiring an elongated morphology and self-organising into the wave-like arrangements characteristic of primary SCs (Supplementary Figure 5A). These TF-induced oSCs were indistinguishable from primary SCs, expressing GFAP and SOX10 at an intensity and with a sub-cellular localisation indistinguishable from that of primary SCs (Figure 5B). Furthermore, they were proliferative and could be stably expanded in culture, demonstrating a complete and sustained fate conversion (Supplementary Figure 5B, C).

A key feature of SC function is their ability to adopt either a myelinating or non-myelinating phenotype, regulated by neuregulin levels. We next tested if the TF-induced oSCs were functionally competent to respond to these cues. Using RT-qPCR, we found that in basal media (lacking neuregulin), TF-induced oSCs expressed markers of immature/non-myelinating SCs (*p75*, *S100b*), but did not express myelination-associated markers (*Pou3f1*, *Krox20*). However, upon treatment with a differentiation factors (neuregulin and cAMP) for 72 hours, the TF-induced oSCs increased expression of *Pou3f1* and *Krox20*, alongside

reduced expression of *p75* and *S100b,* consistent with SC maturation[44]. Notably, differentiated oSCs showed no significant differences from primary SCs across all markers tested (Figure 5C).

The definitive test of SC function is the ability to form peripheral-type myelin. Therefore, as with vitronectin and BMP4-generated oSCs, we next asked whether TF-induced oSCs could myelinate axons *in vitro*. For this, DRG axons were co-cultured with primary or TF-derived oSCs prelabelled with an mCherry lentivirus (Figure 5D). Following the addition of ascorbic acid to promote myelination, the TF-induced oSCs, like primary SCs, successfully aligned with, and ensheathed the DRG axons with the peripheral myelin protein periaxin (PRX) (Figure 5E).

Having established that our TF-induced oSCs phenocopy the morphology and key markers of chemically induced oSCs and primary SCs, we next assessed if this were also true in terms of their transcriptome. We performed single-cell RNA sequencing on the TF-induced population at 5 days post-treatment with lentiviral Sox10 and Olig2-shRNA. This time point was chosen because it represents the earliest appearance of elongated SC-like cells, allowing us to capture cells that still morphologically resemble OPCs and gain insight into the transcriptional networks that drive OPC-to-SC differentiation. At this early time point, unsupervised clustering identified 7 distinct cellular states (Figure 5F). Further RNA velocity analysis using SC embeddings revealed an increased probability for cells in cluster TF1 to differentiate into SCs (Figure 5G). While cells in all clusters expressed a mixture of OPC and SC related genes, cluster TF1 showed the highest expression of SC genes (*Sox10*, *Erbb3*, *Pou3f1*, *Pmp22*, *Gap43*, *Ngfr*) (Supplementary Figure 5D). To determine whether the TF-induced SCs resembled the extrinsic factor induced SCs, we conducted a comparative analysis of the cell-fate driver genes from this dataset and the vitronectin and BMP4-treated cells. The comparison revealed a striking degree of correlation between the cell fate driver genes from the TF-induced cells in comparison to the most mature SC-like cluster from the vitronectin BMP4 treated oSC dataset. A direct differential expression test between the two populations showed no significant differences in key glial identity or maturation genes (Figure 5H).

The comparison revealed that both methods produced cells that ultimately converged on the same mature SC-like transcriptional state. However, trajectory analysis highlighted a notable difference in the efficiency of the conversion. A significantly higher proportion of the TF-induced cells progressed to the final, mature pseudotime state compared to the chemically induced population (Figure 5I). This suggests

that while extrinsic signals like BMP4 initiate the correct program, the direct genetic manipulation of the core SOX10/OLIG2 circuit provides a more potent and deterministic push toward the desired fate. Direct targeting of OLIG2/SOX10 is therefore sufficient to faithfully recreate the complex transcriptional outcome induced by the niche signals.

AAV vector-mediated modulation of Olig2 and Sox10 can increase SC remyelination *in vivo*

To test whether endogenous OPCs could be directed toward a SC fate by modulating the levels of *Olig2* and *Sox10* after *in vivo* demyelination, we generated a dual promoter AAV vector to overexpress *Sox10* and to knock out Olig2 with gRNAs in OPCs using the SOX10-MCS5 promoter (AAV-SOX10/OLIG2KO)[45] (Figure 6A). This vector was delivered intravenously to Cas9 knock-in mice. Control animals were injected with AAV-mKate2, which encodes an mKate2 far-red fluorescent reporter gene[46]. 14 days after AAV delivery, to allow for viral expression, demyelination was induced in the spinal cord white matter by direct focal injection of lysolecithin[47,48]. The resulting lesion is normally remyelinated by both oligodendrocytes and SCs[9], the extent of which was evaluated 28 days post-lesion (Figure 6B).

To distinguish between SCs of endogenous origin generated in response to the lysolecithin lesion from SCs induced from the AAV vector, we fused a HA tag to the SOX10 overexpression cassette or mKate2 fluorescent reporter. Using this system, we confirmed the presence of $HA^+/SOX10^+$ double positive cells as well as $HA^+/SOX10^+/PRX^+$ triple positive cells in both groups (Figure 6C). As expected, HA labelling was restricted to $SOX10^+$ cells, and there was no significant difference in the total number of infected HA^+SOX10^+ cells between the two groups, indicating that both vectors infected OPCs with similar efficiency (Figure 6D). Furthermore, analysis of the overall lesion pathology revealed no significant differences in lesion size (as measured by MBP loss), microglial/macrophage response (IBA1), or overall astrogliosis (GFAP) between the two groups (Supplementary Figure 6A, 6B). Together, this shows that between the two groups, the only significant variable is the genetic manipulation of OLIG2/SOX10 within the infected OPCs cells.

With the model validated, we then quantified the degree of SC conversion within this infected population using the specific SC myelin marker, periaxin (PRX). Animals injected with the AAV-Sox10/Olig2KO showed a significant increase in the number of $HA^+/SOX10^+/PRX^+$ compared to the AAV-mKate2 control group,

confirming increased OPC to SC differentiation in response to the AAV-induced expression of Sox10 and deletion of the Olig2 locus (Figure 6E), providing evidence that the dual genetic manipulation is sufficient to force a cell-autonomous switch from the OPC lineage toward a myelinating SC fate *in vivo*.

Astrocytes and SCs generally occupy non-overlapping domains within the CNS[49]: indeed, astrocytes are a source of SOSTDC1, an antagonist of the BMP/Wnt pathways involved in OPC-to-SC differentiation[16]. We therefore next asked what impact increased OPC-to-SC differentiation during remyelination induced using the dual vector had on the distribution and interactions of these two cell types. We first looked at the total contribution of SC remyelination by quantifying immunoreactivity against peripheral myelin proteins, PRX and myelin protein zero (P0). While PRX^+ (17.07 ± 7.67%) and $P0^+$ (11.92 ± 2.97%) cells were found in control animals (as expected), in animals receiving the AAV-Sox10/Olig2KO, there were significantly more cells that were PRX^+ (34.33 ± 7.39%) or $P0^+$ (30.75 ± 10.13%) (Figure 6F). Consistent with the increase in SC remyelination in mice receiving AAV-Sox10/Olig2KO, we also observed a significant increase in $SOX10^+$ cells, which labels both the oligodendroglial and SC components of remyelination (Figure 6F). We then quantified the spatial relationship between PRX^+ SCs and GFAP+ astrocytes, categorizing each SC as: astrocyte-border, if contacting the edge of a $GFAP^+$ territory; SC-Core, if surrounded only by other PRX^+ cells; or astrocyte-integrated, if located deep within the territory characterised by abundant $GFAP^+$ processes (which were distinguishable $GFAP^+$ non-myelinating SCs). In control lesions, endogenous SCs were restricted to areas in which $GFAP^+$ astrocyte processes were absent, consistent with their established failure to cross the astrocyte boundary[50]. In contrast, treatment with AAV-Sox10/Olig2KO caused a significant decrease in the proportion of cells at the astrocyte-border, alongside a significant increase in the number of astrocyte-integrated cells found within the $GFAP^+$ territory (Supplementary Figure 6C). This enhanced integration of SC within astrocyte-containing regions of the lesion occurred without any corresponding decrease in the overall astrocyte response to demyelination, as the total $GFAP^+$ area was indistinguishable between the control and AAV-treated groups. Thus, cell intrinsic differentiation of OPCs into SCs by transcription factor manipulation can override extrinsic or environmental factors such as the presence of astrocytes that normally suppress this transition.

To confirm that the TF-induced oSCs within the remyelinating lesion were forming myelin sheaths, we performed immunoelectron microscopy to identify HA positive cells. Since SOX10 is fused to a HA tag, we were able to detect, using gold particle conjugated antibodies against HA, immunogold labelling within nuclei of cells with ultrastructural features of SCs. HA-positive cells were observed forming compact, peripheral-type myelin sheaths around host axons, surrounded by a basal lamina, deep within the lesion territory in a 1:1 ratio (Figure 6G).

Identification of oSCs in active MS lesions from post-mortem human samples

Having identified an OPC state primed for SC differentiation in a toxin-induced rodent model of remyelination, we asked whether we could find an equivalent OPC state in humans. For this purpose, we analysed publicly available scRNA-seq data from a study on multiple sclerosis (MS), the most common form of demyelinating disease in the CNS[51] (GEO accession number: GSE279183). We reasoned that in active lesions, in which remyelination is ongoing, the population of OPCs would contain cells at different stages along the differentiation trajectory, possibly including some poised to undergo differentiation into SCs. This dataset was generated from 15 snap-frozen tissue blocks, which included samples from six people diagnosed with MS and seven tissue donors without neuropathology. We extracted 3945 nuclei labelled as OPCs and used scVI to integrate them across donors, leading to new embeddings (Supplementary Figure 7A-D). To identify oSCs based on our *in vivo* injury dataset, we trained a cell type classifier with the cell states identified in our rat remyelination model (Figure 1) using the CellTypist framework[52] (Figure 7A). We found 33 nuclei predicted to be SC-primed OPCs (Figure 7B). These nuclei are shared across three patients with chronic active lesions (MS411 A2A2, MS377 A2D4 and MS377 A2D2) and are co-clustered with nuclei from patients with chronic active lesions (Figure 7C, Supplementary Figure 7B). These predicted oSCs also express SC-related genes including (*Sox10*, *Erbb3*, *Pmp22*, *Scn7a*). (Figure 7D and Supplementary Figure 7E). To further compare these predicted oSCs to SC and OPCs, we calculated an OPC score and a SC score, which consist of well-established marker genes (Table S3). Consistent with our marker gene analysis (Figure 7F), we found that the predicted oSCs have a higher SC gene score (Figure 7D, left) and a lower OPC gene score (Figure 7D, right) than all other OPCs. Since we observed that predicted oSCs are only present in patients with active lesions, we analysed the SC gene score in all OPCs stratified by lesion type. We found that there is a significant increase in SC scores in nuclei

from donors with chronic active lesions compared to control nuclei (Figure 7E and Supplementary Figure 7F). Consistently, OPC gene scores were also significantly decreased in chronic active lesions compared to controls (Supplementary Figure 7G, upper panel). There was no significant difference between groups in oligodendrocyte gene scores (Supplementary Figure 7G, lower panel).

Beyond gene markers, we investigated the cellular programmes of these putative MS-related oSCs. We found that these patient-derived oSCs are also characterised by increased integrin signalling (Figure 7G) and higher expression of the same top transcription factors (Figure 7H) as found in the animal injury data (Figure 1G). Since we showed that activation of integrin signalling is necessary for OPC-to-SC transition (Figure 2), we sought to identify which cells could contribute to integrin signalling OPC-to-SC transition. Using unbiased cell-cell communication analysis via CellPhoneDB[53], we found that multiple cell types, including stromal cells, neurons, astrocytes and oSCs themselves, can signal to oSCs via integrin signalling (Figure 7I and Supplementary Figure 7H). We conclude that oSCs can be found in active human MS lesions and have similar transcriptomic characteristics to OPC-derived SCs from animal models.

DISCUSSION

The generation of SCs, cells normally of neural crest origin from OPCs, cells of neuroepithelial origin, during spontaneous CNS remyelination represents a unique example in vertebrates of an adult stem cell spontaneously generating a cell type derived from a separate germ layer origin during tissue regeneration. Earlier reports of adult stem cells giving rise to differentiated cells of a different germ layer origin, such as tail regeneration in urodele amphibians or mammalian bone marrow stem cells giving rise to organs of ectodermal origin are unreliable because of the confounding effect of cell fusion[2]. The nature of this process makes it difficult to define by pre-existing terminology. Two related theoretical regeneration frameworks exist that resemble the OPC-to-SC differentiation phenomenon: de-differentiation and transdifferentiation. Dedifferentiation entails the reversion of a differentiated cell into a stem cell state, such as occurs in the intestine after ablation of the $LGR5^+$ adult stem cell population, after which more differentiated cells can (re-)gain stem cell potential and populate the stem cell niche[54,55]. Examples of transdifferentiation, the generation of a differentiated cell from another differentiated cell, include the conversion of alpha into beta cells during pancreas regeneration[56], and occur between developmentally closely related cell lineages of the same germ layer. In the process we describe here, we do not find OPCs dedifferentiating into a common progenitor of the neural ectoderm and neural crest lineages. The differentiation of OPCs into SCs resembles features of transdifferentiation, as it occurs without stable intermediate stages - a process commonly achieved by the enforced expression of transcription factors. Recent studies identify adaptive cellular reprogramming, a mechanism where injury triggers a radical change in the identity of differentiated cells *in vivo.* This process promotes tissue repair by generating a transient class of repair cells or by directly replacing cells lost during tissue damage[57]. The conversion of myelinating SCs to repair SCs in the peripheral nerve is a prime example of generating this transient repair cell state[58]. The differentiation of OPCs into SCs aligns with this broader adaptive framework as it represents an injury-induced change in cell fate to achieve repair. However, OPCs represent a population of adult progenitor cells, not a differentiated cell type in the conventional sense of the term, making this a unique phenomenon not covered by existent terminology, even within the adaptive cellular reprogramming context

This form of SC-mediated, OPC-derived remyelination is especially unusual given the early developmental divergence of the neural crest from the neuroepithelium at the time of gastrulation, occurring between

embryonic days 6 and 9 in mice and at around 3 weeks in humans. The phenomenon of OPC-to-SC differentiation thus challenges the rigidity of developmental boundaries, demonstrating that glial identity can be more fluid than previously appreciated. The divergence between SCs and the neuroepithelium also likely occurs early on in evolutionary terms, since distinct modes of CNS and PNS myelination are apparent in the most primitive myelinated vertebrates (Chondrichthyes)[16]. In this study, we provide insights into how this regenerative plasticity in OPCs comes about, establishing mechanisms, both extrinsic and intrinsic, that differentiate OPCs into SCs using a combination of vitronectin and BMP4, via the modulation of two transcription factors, OLIG2 and SOX10. Since both vitronectin and BMP4 are abundant in the injured CNS, our findings suggest a physiologically relevant mechanism for OPC-derived SC differentiation during CNS myelin regeneration.

Under homeostatic conditions, BMP signalling is, in part, regulated by astrocyte-derived BMP antagonists such as SOSTDC1, which favor oligodendrocyte differentiation while preventing OPC conversion into SCs or type II astrocytes[22,59]. However, in some demyelinating lesions astrocytes are lost or are dysfunctional, resulting in this inhibition being lifted, and thereby leading to unopposed BMP signalling[60]. Our findings suggest that elevated BMP activity destabilises oligodendroglial lineage commitment through the loss of OLIG2, placing OPCs in a transiently plastic state. In the presence of ECM components such as vitronectin, likely mediated by integrin signalling, these OPCs then initiate a transcriptional program leading to SC differentiation. Without additional cues, BMP alone is insufficient to induce SC differentiation, and, at least *in vitro,* the default differentiation pathway of OPCs is into astrocytes.

The presence of integrin signalling appears to be a critical determinant of OPC-to-SC conversion. Vitronectin, a plasma-derived ECM protein, binds integrin receptors to modulate key intracellular pathways, including PI3K, JNK, and RAC1, which influence adhesion, survival, and differentiation[24]. Importantly, OPCs exclusively express αV-family integrin receptors capable of binding vitronectin during remyelination[61]. Our transcriptomic analysis revealed the upregulation of integrin-related genes (*Itga1*, *Itga6*, *Itga8*, *Itgb4*) in OPC-derived SCs, reinforcing their role in SC differentiation. Interestingly, integrin signalling during SC development is highly context-dependent: αV activation recruits the SRC-family kinase LYN to maintain the progenitor state, whereas activation of SFK FYN promotes oligodendrocyte differentiation and myelin gene expression[62]. Our findings suggest that during injury, integrin signalling

shifts OPC differentiation toward an SC fate by modulating SOX10 activity and stabilizing SC lineage gene expression.

In terms of the expression of transcription factors involved in regulating cell fate and maintenance, BMP and integrin signalling converge to regulate OPC fate via OLIG2 and SOX10. Under normal conditions, OLIG2 binds SOX10 to maintain oligodendroglial gene expression while actively repressing SC differentiation factors such as POU3F1 and KROX20[63]. BMP signalling disrupts this balance by blocking OLIG2 activity[23,34], lifting repression of SC-related genes. However, BMP signalling without integrin activation leads to astrocyte differentiation[64]. Our results reconcile these findings by demonstrating that SOX10 must remain active to drive SC gene networks. In this regard it is intriguing that fibronectin was able to act synergistically with Sox10 during fibroblast to neural crest stem cell transdifferentiation, an effect that was lost in the presence of BMP pathway inhibitors[65]. Bioinformatic analysis identified direct SOX10-mediated regulation of genes involved in collagen synthesis and cytoskeletal remodeling, key pathways for SC differentiation. Thus, integrin signalling may help to stabilise SOX10 levels in the injury niche, allowing for a shift in transcriptional partnerships—from OLIG2-SOX10 to SOX10-POU3F1 interactions—thereby facilitating SC fate acquisition.

It is unclear what the functional advantage, if any, of SC-mediated remyelination in the CNS might be and why it might have evolved. One can nevertheless speculate on what its translational benefits might be. In terms of MS, a disease involving the autoimmune targeting of CNS myelin epitopes, remyelination with peripheral-type myelin that produced by SCs would result in repair that is unlikely to be susceptible to further immune attack, given that there is no PNS component of MS. Thus, promoting SC remyelination would likely be sustained and impervious to the disease process. In experimental models, SC remyelination appears to occur more rapidly than oligodendrocyte remyelination [66] and might therefore reduce the time an axon remains demyelinated when it is likely to be at its most vulnerable. In traumatic injury to the CNS, there is a failure of axon regeneration in large part due to the presence of axon growth inhibitory molecules expressed by oligodendrocytes and their myelin, such as NOGO [67] and MAG [68]. SCs, in contrast, are highly supportive of axon regeneration [69] and therefore, although primary demyelination generally represents a small component of the overall pathology of traumatic injury, promoting PNS rather than CNS remyelination would result in an environment generally more conducive to regeneration. More ambitiously, one could imagine that diverting OPCs towards SC remyelination might have value in

genetic disorders caused by mutations in genes expressed exclusively in oligodendrocytes. In each of these potential scenarios an obstacle has always been the mutual exclusivity of SCs and astrocytes, especially the reactive astrocytes that are a near-ubiquitous feature of many CNS pathologies [70,71]. However, in this study we show that by targeting the transcriptional machinery by which OPCs become SCs, it is possible to bypass environmental inhibitory signals for SCs and create areas of SC (re-)myelination in which astrocytes are also present, thereby offering new strategies for remyelination therapies by biasing OPC fate choices.

Limitations of the study

In this study we provide evidence that ECM molecules, vitronectin (and fibronectin), alongside BMP signalling, can induce OPCs to differentiate into SCs. However, our current methodology does not allow us to pinpoint the specific, critical ECM molecule or the exact combination of ECM-derived integrin signalling required to fulfill this function in either our animal model or in a clinical setting. Assessing this through genetic deletion is challenging, given the high redundancy and widespread presence of ECM molecules and the complex convergence of integrin signalling pathways derived from multiple sources. To circumvent this methodological difficulty and to identify the functional outcome of the combined signalling, our strategy focused on identifying the downstream transcriptional events. Our results successfully show that the combination of integrin and BMP signalling acts to stabilise SOX10 levels, while reducing OLIG2. The consequence of lowering OLIG2 is critical to push OPCs of their canonical oligodendroglial lineage, so allowing the alternative SC fate to be established. Therefore, while the precise initiating ECM ligands remain to be fully deconvoluted, the current study provides robust evidence for the transcriptional mechanism by which this extrinsic signalling drives OPC to SC differentiation.

An interesting question, beyond the bounds of the current study, is whether there are meaningful functional consequences for a CNS axon whether it is myelinated by an oligodendrocyte or by a SC. While both cell types form myelin, the fundamental differences in their basal lamina composition, node of Ranvier structure, and maintenance processes could differentially impact long-term axonal stability and conduction velocity. Additionally, the potential therapeutic benefit of SC remyelination may be anatomically restricted. The axonal diameter threshold for myelination differs significantly between the CNS (approximately 0.2 µm), and the PNS (1 µm). Consequently, the benefits of SC remyelination [72] may

only be realised in areas with larger diameter axons, necessitating careful consideration for clinical translation. Nevertheless, the current study provides a knowledge base from which many subsequent studies on this unusual phenomenon can be explored.

CODE AVAILABILITY

All code is available in our GitHub repository (https://izu0421.github.io/opc2sc).

DATA AVAILABILITY

The single-cell RNA data have been deposited at the ENA with dataset identifier *******.

CONFLICT OF INTEREST

Y.Y. is a founder and holds equity in Healthspan Biotics.

AUTHOR CONTRIBUTIONS

Conceptualisation, C.Z.C., B.N., R.J.M.F.; Methodology, C.Z.C., N.M., Y.Y, B.N.; Investigation and data analysis, C.Z.C., N.M., Y.Y., J.F.C., K.S.R., C.Z., M.H., B.N.; Writing C.Z.C., B.N., R.J.M.F.; Funding Acquisition R.J.M.F.; Supervision, P.A-F., B.N., R.J.M.F.

ACKNOWLEDGEMENTS

C.Z.C. was supported by a Wellcome Trust PhD fellowship. N.M. was supported by the Sackler Trust. B.N. was supported by a Kim and Julianna Silverman research fellowship. K.S.R was supported by a Banting Postdoctoral Fellowship from the Canadian Institute of Health Research as well as a Multiple Sclerosis Society of Canada Fellowship. R.J.M.F. is supported by funding from the UK Multiple Sclerosis Society (MS50) and Dr Miriam and Sheldon G Adelson Medical Research Foundation, and a core support grant from the Wellcome Trust and MRC to the Wellcome Trust-Medical Research Council Cambridge Stem Cell Institute (203151/Z/16/Z). We thank Gemma Cronshaw for performing the tail vein injections, Maike Paramour and Laura Everton for generating the 10X sequencing libraries. We thank Karin Müller and Louis Elfari (University of Cambridge Stem Cell Institute, for their assistance with the immunoelectron microscopy.

METHODS

Animal Husbandry

All procedures were performed in compliance with the rules and regulations of the UK Home Office and were approved by the University of Cambridge Animal Welfare and Ethical Review Body. Animals were housed in groups of up to 4 animals and kept at a 12-hour dark-light cycle with free access to standard chow and water. Animals were randomly allocated to experimental groups, which were matched for age and gender.

Isolation and culture of oligodendrocyte progenitor cells

Primary OPCs were isolated from neonatal (P2-P10) or young adult (8-24 week) male and female Sprague Dawley rats. The brains were diced with a scalpel into 1 mm^3 pieces. The tissue pieces were digested in Hibernate A Low Fluorescence (HALF, #HALF500) solution containing 34 U/mL papain (Worthington, #LS003127) and 40 µg/mL DNase I (Sigma, #D5025) on an orbital shaker (55 rpm) for 40 min at 37°C. The tissue was centrifuged then resuspended in HALF supplemented with B27 (1:50; Gibco #17504044) and sodium pyruvate (2 mM; Gibco #11360070). To obtain a single cell suspension, the tissue was triturated 10 times each using a 5 mL serological stripette, and 3 fire-polished pipettes of decreasing diameters. The supernatant, containing the cells, was filtered through a 70 µm cell strainer into a tube containing 22.5% isotonic Percoll (GE Healthcare, #17-0891-01) in DMEM/F12 (Gibco, #31331028). The single cell suspension was then separated from tissue and myelin debris by gradient density centrifugation at 800 g (without brakes) for 20 min at RT. The resulting cell pellet was resuspended in red blood cell lysis buffer (1 mL, BD Biosciences, #555899) for 1 min to remove contaminating red blood cells. Subsequently, the cell suspension was incubated in Miltenyi washing buffer (MWB; 2 mM EDTA, 2 mM sodium pyruvate, 0.5% BSA) and 1.7 µL mouse-anti-rat-A2B5-IgM antibody (Merck Millipore, #MAB312) for each adult brain, or 0.25 µL antibody for each neonate brain for 15 min at 4°C. After incubation, cells were washed with 7.5 mL MWB and centrifuged (300 g, 5 min, RT). The pellet was resuspended in 80 µL MWB-insulin, containing 20 µL rat anti-mouse IgM magnetic beads (Miltenyi, #130-047-302) for 15 min at 4°C. The secondary antibody was diluted in 7 mL MWB buffer and centrifuged (300 g, 5 min, RT). After the spin, cells were resuspended in 0.5 mL MWB-insulin, then transferred into the MS-column. The column was washed three times with 0.5 mL MWB-insulin per wash, then discarded. To collect the $A2B5^+$ bound fraction, the MACS MS column was removed from the magnetic stand, and cells were eluted with 1 mL OPC medium (60 µg/mL N-Acetyl cysteine (Sigma, #A7250), 10 µg/mL human recombinant insulin (Gibco, #12585014), 1

mM sodium pyruvate (Gibco, #11360070), 50 µg/mL apo-transferrin (Sigma, #T1147), 16.1 µg/mL putrescine (Sigma, #51799), 40 ng/mL sodium selenite (Sigma, #214485), 60 ng/mL progesterone (Sigma; P0130), 330 µg/mL bovine serum albumin (Sigma, #A4919). Cells were counted, then 20,000 cells/cm^2 were plated onto poly-D-lysine (5 µg/mL PDL; Sigma)-coated glass bottom well plates and incubated in OPC medium supplemented with b-FGF (20 ng/mL; Peprotech, #100-18B) and PDGF (20 ng/mL; Peprotech, #100-13a) at 37°C, 5% CO_2, 5% O_2. Counts averaged 1.2 x10^6 OPCs per brain. The morning after isolation, the OPC proliferation medium was completely replaced to remove any dead cells. Whilst in culture, two-thirds of the media was replaced every 48 h with growth factors added freshly per media change. Cells were allowed to recover for up to 72 h after isolation in proliferation media before treatment with small molecules, lipofectamine transfection or viral infection.

Isolation and culture of Schwann cells

SCs were obtained from the sciatic nerve of 1-2 day old Sprague Dawley rat pups. Briefly, sciatic nerves were dissected and immediately submerged in HALF isolation medium. The epineurium was removed, and the peeled nerves were teased until the fascicles were separated and cloudy. The nerves were transferred to a fresh tube containing cold HALF solution and collected by centrifuging for 5 min at 300 g at RT. The tissue was then digested in collagenase type 1 (2 mg/mL; Sigma, #C0130) and trypsin (1.25 mg/mL, Sigma, #T9201) diluted in HALF at 37°C for 45 min. To obtain a single cell suspension, the nerves were mechanically dissociated by triturating with a P1000 pipette. Cells were centrifuged (3 min, 300 g, RT), and then seeded onto laminin (Sigma, #L2020)-coated well plates with fresh D-media (DMEM media supplemented with 10% FBS) and left to recover in the incubator overnight (37°C, 5% CO_2). The following day, cultures were treated with cytosine arabinoside (Ara-C; 10 µM; Sigma, #C6645) diluted in D-media for 2 days to suppress growth of fibroblasts. Subsequently, the Ara-C containing media was removed, and the cells were allowed to recover and expand for 2 days in normal D-media. The remaining fibroblasts were eliminated by complement-mediated killing using the IgM class anti-Thy1.1 antibody (1:500; Serotec, #MCA04G) and rabbit complement (Millipore, #234400). To promote SC expansion, the cultures were switched onto SC growth media containing DMEM supplemented with 10% FBS, neuregulin (10 ng/mL, Peprotech, #396-HB), forskolin (2 µM; Sigma, #F6886), and 1% penicillin/streptomycin. Cells were cultured at 37°C, 5% CO2 and fed every 3 days. After reaching 80% to 90% confluency, SCs were trypsinised with 0.25% Trypsin-EDTA, centrifuged (5 min, at 300g, RT) and passaged.

Isolation and culture of dorsal root ganglion (DRG) cells

DRGs were collected from the spinal columns of E14 rat pups and transferred into a 6 cm sterile dish containing 1 mL ice-cold HALF. Then the DRGs were transferred into a falcon tube containing 2.5 mL 0.025% trypsin dissolved in Ca^{2+} and Mg^{2+}-free PBS (Sigma, #T9201) and incubated at 37°C for 20 min on an orbital shaker. Afterwards, the ganglia were further digested in 600 µL type I collagenase solution (1.5 mg/ml; Sigma, #SCR103) at 37°C for 30 min on an orbital shaker. Subsequently, DMEM with 10% FBS was added to terminate the digestion, and the cell pellet was collected by centrifuging for 5 min at 300 g at RT. To obtain a single cell suspension, the cell pellet was mechanically dissociated by triturating with a P1000 pipette. Cells were centrifuged (3 min, 300 g) and then seeded onto laminin coated well plates with serum free DMEM (DRG media) containing 50 ng/mL NGF (R&D systems, #256-GF), N2 supplement (1:50, Gibco, #17502048) and 0.05% BSA, and left to recover in the incubator overnight (37°C, 5% CO_2). The following day, cultures were treated with Ara-C (10 µM; Sigma) diluted in fresh media for 2 days to suppress growth of fibroblasts and SCs. Subsequently, the Ara-C containing media was removed, and the cells were allowed to recover and expand for 2 days in normal media. Cultures were cycled through Ara-C mediated elimination of nonneuronal cells at least three times to obtain purified neuronal cultures.

Once the DRG neurons were purified, SCs, prelabelled with a PGK-H2B-Cherry (Addgene plasmid #21217) lentivirus, were trypsinised, then seeded with DRGs at a density of 2×10^5 cells/400 µL. DRG-SC co-cultures were maintained in DMEM (Gibco, #D5796) supplemented with 10% FBS, Glutamax (2mM, Gibco), NGF (50 ng/mL NGF) and penicillin-streptomycin (C media). After 7 days, ascorbic acid (50 µg/mL) was added to the C medium to induce myelination. Cells were maintained at 37°C, 5% CO_2 with media changes every 2 to 3 days.

shRNA-lentivirus mediated deletion of Olig2

Oligonucleotides encoding the *Olig2* shRNA sequence (Fwd: GATCCGTTCTTGTGTGTGTAAATATAAC TCGAGTTATATTTACACACACAAGAACTTTTTG; Rev AATTCAAAAAGTTCTTGTGTGTGTAAATAT AACTCGAGTTATATTACACACACAAGAACG) were oligoannealed, then ligated into the pGreenPuro-shRNA-Stx3S-C4 (Addgene #99742) using a T4 ligase (New England Biolabs). The sequences were confirmed with Sanger sequencing, then plasmids were transformed into Stable Competent *E.coli* (New England Biolabs, #C3040H) and purified with the NucleoBond Xtra MIDI kit (Machery-Nagel, #11932492).

To generate shRNA lentiviruses, HEK293T cells were grown in 15-mm plastic dishes and triple-transfected with the pMD2.G envelope plasmid (Addgene plasmid #12259), the psPAX2 packaging plasmid (Addgene plasmid #12259), and the transgene plasmid. Viral supernatant was collected at D3 and D5 post

transfection, then concentrated using the Lenti-X Concentrator (TakaraBio, #631232) as per manufacturer's instructions. Purified lentiviruses were aliquoted and stored at -80°C until required. To knockdown *Olig2*, OPC cultures were treated with purified shRNA-lentivirus diluted in 500 µL of OPC media containing growth factors (PDGF and FGF) for 48 h.

Construction of gRNA and overexpression plasmids

Two AAV plasmids were generated using PCR to amplify fragments containing appropriate overlaps, followed by Gibson assembly using the NEBuilder® HiFi DNA Assembly Master Mix (NEB, #E2621S). Detailed plasmid maps and cloning primers are provided in the supplementary GenBank files.

1.AAV-TRE-HA-Sox10-gRNA-Sox10U2PROM-rtTA-WPRE

This construct was assembled from elements derived from several templates, including: an AAV backbone (from AAV-CMVc-Cas9, Addgene #106431), a TRE promoter (from LV-pInducer20, Addgene #44012), and an HA-tagged Sox10 coding sequence (from Tet-O-FUW-Sox10, Addgene #45843). It also includes a synthetic gRNA expression cassette containing the first 110 bp of the mouse MALAT1 triple helix[64], the Hammerhead and HDV ribozymes[73], two *Olig2* targeting gRNAs (Olig2_gRNA1: ACGATGGGCGACTAGACACC, Olig2_gRNA2: GCACGACCTCAACATCGCCA) separated by a pre-tRNA-Gly sequence and a polyadenylation signal. The Sox10 U2 promoter (from LV-Sox10MCS5-GFP, Addgene #115783) and an rtTA-WPRE module (from pHR-EF1α-Tet-on 3G, Addgene #118592) were incorporated to enable doxycycline-dependent HA-Sox10 induction.

2.AAV-Sox10U2PROM-rtTA-T2A-mKate2-WPRE

A second construct was generated using the same AAV backbone (AAV-CMVc-Cas9, Addgene #106431) and Sox10 U2 promoter, combined with rtTA, a T2A self-cleaving peptide, and WPRE elements (from pHR-EF1α-Tet-on 3G), together with mKate2 (from NFKBRp-mKate2-2xNLS-p2a-puroR, Addgene #82024) to enable fluorescent reporting of promoter activity.

AAV Production

AAVs were produced and purified as described in[74] . Briefly, HEK293T cells were grown in 15-mm plastic dishes and triple-transfected with the pHelper plasmid (Addgene plasmid #112867), the PHP-EB capsid plasmid (Addgene plasmid #103005), and the transfer plasmid. Virus particles were isolated by ultra-centrifugation (350,000 g) of the supernatant collected at D3 and D5 post transfection, as well as lysed cells collected at D5 post transfection using an Optiprep density-gradient medium (Sigma; #D1556).

Following ultra-centrifugation, the viral layer was extracted, then concentrated using Amicon Ultra-15 centrifugal filter units (Sigma; #Z648043-24EA). The AAV titre was determined using SYBR Green qPCR and stored at 4°C until use.

Induction of white matter lesions and Schwann cell transplantation in the brain

Adult female Sprague Dawley rats (12-20 weeks) were anesthetised with buprenorphine (0.03 mg/kg, s.c.) and 2.5% isoflurane. Then, bilateral demyelination was induced by stereotaxic injection of 4 µL of 0.01% ethidium bromide (EtBr) into the caudal cerebellar peduncles (CCPs), as previously described (Woodruff and Franklin, 1999). The EtBr was delivered at a rate of 1 µL/min. 7 days later, 300,000 SCs pre-labelled with PGK-H2B-mCherry lentivirus (Addgene plasmid #21217) in 4 µL of $HBSS^{-/-}$ were transplanted unilaterally into the ethidium bromide-induced area of demyelination in the left CCP.

AAV delivery and spinal cord lesioning

5 X 10^{11} viral genomes of each AAV were tail vein injected into adult (8-12 weeks) ROSA-26-Cas9 (The Jackson Laboratory, #026179). To induce transgene activation, animals were switched onto water containing Ribena and doxycycline (2 mg/mL, Sigma, #D9891) from D10 to D14. Animals also received a one-time intraperitoneal injection of doxycycline on D11 (5 mg/ml, diluted in saline solution). 10 days after AAV delivery, spinal cord lesions were induced by injecting 1 µL of 1% lysolecithin (Sigma, #L4129) between two vertebrae of the thoracic column into the ventral funiculus at a rate of 1 µL per minute as previously described[75]. After lysolecithin delivery, the needle remained in position for an additional minute to prevent backflow of the lysolecithin solution.

Perfusion and tissue processing for immunohistochemistry

Adult mice or rats were transcardially perfused with 0.9% NaCl solution for 1 minute, followed by 4% freshly depolymerised paraformaldehyde (PFA) in PBS for 7 minutes. The spinal cord and brain were dissected out then post-fixed in 4% PFA at 4°C overnight. Tissues were cryoprotected in 30% sucrose solution overnight, embedded in OCT medium (TissueTek, #4583), then cut into 12 µm thick sections using a cryostat.

Immunohistochemistry of tissue slides or cultured cells

Non-specific antibody interactions were blocked by incubating tissue slides in blocking solution containing 10% donkey serum (Sigma, #D9663), 1% bovine serum albumin, 0.1% cold fish gelatin (Sigma, #G7041),

0.1% Triton X-100 (Sigma, #T8787) and 0.05% Tween20 (Sigma, #P9416) in PBS for 30 to 60 min at RT. Primary antibodies (Table S1) were diluted in 5% donkey serum in PBS and incubated overnight at 4°C. The slides were washed 3 times for 5 min with PBS, then incubated in secondary antibodies (Table S1) diluted in 2% donkey serum in PBS (1 h, RT). Subsequently, nuclei were counterstained with DAPI (1:10,000) in PBS for 10 min, then washed 2 times with PBS for 5 min. The slides were mounted onto coverslips using Fluromount mounting media (Sigma, #F4680).

Similarly, cultured cells were washed with PBS containing Ca^{2+} and Mg^{2+} twice before fixation with 4% PFA for 15 min at RT. Subsequently, the cells were washed with 1X PBS three times (5 min, RT, shaking), blocked and permeabilised with 10% PBS-T (with 0.1% Triton X-100) for 30 min, then stained using the same protocol. Images were acquired using a confocal microscope (Leica TCS SP8, Zeiss LSM 980 Airyscan, or Zeiss Axioscan 7) and processed using ImageJ or QuPath. Cell populations were quantified manually from at least 3 fields of view per biological replicate.

Perfusion and tissue processing for immunoelectron microscopy

Adult mice or rats were perfused transcardially with 0.9% NaCl solution for 1 minute, followed by a 6-minute perfusion of 4% freshly depolymerised PFA in PBS. The spinal cord was carefully dissected and post-fixed overnight at 4°C in a solution containing 2% PFA and 2% glutaraldehyde in PBS. After fixation, tissues were embedded in 10% gelatin (Sigma; #48724) and sectioned into 1 mm thick slices using a vibratome. These sections were further post-fixed in 4% PFA for 15 minutes, then blocked with a blocking buffer for 24 hours at 4°C.

Next, the tissues were incubated with the HA primary antibody (Invitrogen, #26183) at 4°C for 96 h. Following primary antibody incubation, the sections were treated with an immunogold secondary antibody (1:20; Sigma; G7652) for 24 h at 4°C. After staining, the immunogold signal was further developed using a silver enhancer kit (Sigma, #SE100) as per the manufacturer's instructions. Stained sections were sections osmicated overnight at 4°C in a 0.25% osmium solution then dehydrated in an ascending ethanol series and propylene oxide then embedded in resin (TAAB). For electron microscopy analysis, ultrathin sections (70 nm) from the lesion sites were cut and transferred onto copper grids. These sections were stained with lead citrate, and grids were visualised using a Hitachi-HT7800 transmission electron microscope.

RNA isolation and qRT-PCR

RNA was isolated from cultured OPCs using the Directzol RNA MicroPrep Kit (Zymo, #R2050). cDNA was generated using the QuantiTect Reverse Transcription Kit (Qiagen, #205311). For quantitative real-time (qRT)-PCR, PowerUp SYBR Green master mix (Applied Biosystems; #A25742), primers (500 mM, Table S2), RNAse-free water, and cDNA were loaded according to manufacturer's instructions. Each reaction was repeated in duplicate. Subsequently, RT-qPCR and melting curve analysis was performed on Life Technologies Quantstudio 6 Flex Real-Time PCR System. Fold changes in gene expression were calculated using the Livak method[76].

Western blot

Cells were lysed in RIPA lysis buffer (Sigma, #R0278) supplemented with 1% Halt protease and phosphatase inhibitor (Thermofisher, #78442) for 30 min on ice. The lysates were centrifuged for 30 min at 4°C at 13,000 g in a tabletop centrifuge. The supernatant was stored at 80°C. Protein quantification was carried out using the Pierce BCA protein assay kit (Thermofisher, #23209) measured with the SPECTROstar Nano absorbance plate reader.

For normal western blot, protein lysate was mixed with 4X NuPage LDS Sample Buffer (Thermofisher, #NP0007) and 10X NuPage Sample Reducing Agent (Thermofisher, #NP0009), then incubated at 70°C for 10 min. 50 µg of each protein sample were loaded per well, then separated on Bolt 4%–12% Bis-Tris Plus gels (Thermofisher, #NP0322PK2) in Bolt MOPS SDS running buffer (Thermo Scientific, #B000102) supplemented with 1 ml NuPage antioxidant (Thermofisher, #NP0005) at 150 V for 60 min. Subsequently, the protein was transferred to a polyvinylidene fluoride (PVDF, Immobilon, #IPFL00010) membrane in NuPage transfer buffer (Thermofisher, #NP0006) for 60 min at 20 V using the Mini Blot module (Thermo Scientific). After protein transfer, membranes were blocked in Intercept TBS blocking buffer (Li-COR, #927-60001) for 1 h at RT, then incubated in blocking buffer containing 0.1% Tween20 (TBS-T) containing primary antibodies on a shaker overnight at 4°C. The membranes were washed thrice in TBS-T for 5 min, and then incubated in secondary antibody diluted in blocking buffer, at RT for 1 h. After incubation, the membranes were re-washed three times in TBS-T and imaged using the Odyssey (Li-Cor).

For Jess Simple Western, protein lysates were diluted to a final concentration of 0.5 mg/mL, then all samples, and buffers were loaded into the cartridges as according to the manufacturers' instructions.

SOX10 (Abcam, #AB155279) was used at a concentration of 1:50, and bActin (Cell Signalling, #3700) was used at a concentration of 1:250 in Antibody Diluent 2 (Bio-Techne, #042-203).

Generation of single-cell RNA sequencing data for Smart-seq2

Focal white matter demyelination was induced unilaterally in the caudal cerebellar peduncle of adult female rats (12 weeks) using 0.01% ethidium bromide. 10 days post lesion, both the lesioned and contralateral uninjured CCP were microdissected, and A2B5$^+$ cells were isolated using FACs. This timepoint corresponds to the onset of OPC differentiation in the EtBr-CCP lesion[75]. Sequencing libraries were prepared using a modified Smart-seq2 protocol[77] and sequenced using the Illumina HiSeq 4000. Reads were aligned to the rat genome (Rattus_norvegicus Rnor_6.0.88).

Generation of single-cell RNA sequencing data for 10X genomics

TF-induced OPC-derived SCs and Vn/BMP4-induced OPC-derived SCs were detached from culture plates using TrypLE Express (Gibco, #12604013) then 10,000 cells per sample were submitted to the Cambridge Stem Cell Institute Genomics core for RNA isolation and library preparation. Individual cells were partitioned into Gel Bead-In-Emulsions (GEMs) in accordance with the Chromium Single Cell 3' protocol (10X Genomics, #120237). Briefly, the single cell GEMs were dissolved, which releases and allows mixing of the cell lysate with a primer pool containing an Illumina Read 1 sequence, a 16 nt 10x Barcode, a 10 nt Unique molecular identifier, and a poly-dT primer sequences). Incubation in this reverse transcription master mix yields barcoded, full-length cDNA. The GEMs were lysed, PCR amplified, and the quality of the cDNA was assessed using high sensitivity DNA electrophoresis (Agilent Technologies, #5067-4626) with the Agilent bioanalyzer system. Illumina-compatible cDNA libraries were prepared for sequencing using single cell the Single Cell 3' Reagent kit protocol. Sequencing was performed on the Illumina NovaSeq 6000 S2. The number of assigned reads for each sample was between 362 million and 666 million, with a minimum read depth of 40,955 reads per cell. After sequencing, FASTQ files were mapped to the rat reference genome (RGSC6.0/rn6) using Cellranger v5.0.1 and processed on Scanpy.

Analysis of single-cell RNA sequencing data

The analysis of single-cell RNA sequencing data was performed similarly to previous work[78]. For the *in vivo* data, low-quality cells were removed based on predefined filtering criteria, and subsequent steps were taken to correct for technical variations in the dataset according to best practices[79]. Specifically, total counts, the percentage of mitochondrial counts, and the percentage of External RNA Controls Consortium

(ERCC) spike-in counts were regressed out to normalise the data and mitigate technical confounding effects. The preprocessing steps and scripts used are available at dataset preprocessing and removal of low-quality cells and regressing out unwanted variables. Following preprocessing, cell states, also referred to as cell types, were annotated. This annotation was performed using marker-based identification to ensure accurate classification of distinct cell populations. The full annotation workflow can be accessed via our cell state annotation script.

To investigate the dynamics of OPCs in both injured and control conditions, cell trajectory analysis was conducted using Partition-based Graph Abstraction (PAGA)[20]. This approach allowed for the reconstruction of differentiation trajectories, capturing the progression of OPC states across conditions. The full analysis pipeline for PAGA trajectory inference is available at PAGA trajectory analysis. In addition to trajectory inference, cell fate mapping was performed using CellRank, which employs probabilistic modeling to infer the future states of cells based on transcriptomic similarities. The methodology for cell fate inference using CellRank is detailed at cell fate mapping via CellRank. Transcription factor enrichment analysis was performed using ChEA3[80] and pathway enrichment using STRING[81].

For both BMP-treated OPCs and those subjected to Sox10 overexpression or Olig2 shRNA knockdown, preprocessing steps included quality control, filtering of low-quality cells, and normalization of gene expression counts using similar pipelines (BMP-treated QC, TF-perturbed QC). To assess transcriptional dynamics, RNA velocity analysis was performed using scVelo to infer the future states of cells based on spliced and unspliced mRNA kinetics (BMP-treated RNA velocity, TF-perturbed RNA velocity). Cell fate mapping was then conducted with CellRank to predict differentiation trajectories influenced by BMP signalling or transcription factor perturbations (BMP-treated CellRank, TF-perturbed CellRank).

For the analysis of human multiple sclerosis snRNA data, count matrices from Lerma-Martin and colleagues[51] were downloaded. Nuclei labelled as OPCs by the original authors were extracted, preprocessed, and re-integrated using scVI[82]with the donor, number of genes by counts and percentage of mitochondrial counts as continuous variables. For the identification of oSCs in human OPCs, we first trained a model using CellTypist[52,83] from the rat demyelination single cell data, and used label transfer to predict the putative oSC in samples from human MS patients. Pathway and transcription factor analyses were performed as described above, and cell-cell communication analysis was done using CellPhoneDB[84].

Statistical analysis

Statistical analyses were performed using R and GraphPad Prism. Prior to data analysis, Shapiro-Wilk tests were performed to confirm normality of the data. The data are presented as the mean values, and the error bars indicate ± standard deviation (s.d.). The number of biological replicates per experimental variable (n) is indicated in either the respective figure or figure legend. Blinding was not performed. Significance is indicated as *$p<0.05$, **$p<0.01$, ***$p<0.001$, ****$p<0.0001$ and not significant (n.s.) for $p>0.05$.

REFERENCES

1. Rinkevich, Y., Lindau, P., Ueno, H., Longaker, M.T., and Weissman, I.L. (*2011*). Germ-layer and lineage-restricted stem/progenitors regenerate the mouse digit tip. Nature *476*, 409*–413*. https://doi.org/*10*.1038/nature10*34*6.

2. Wagers, A.J., and Weissman, I.L. (2004). Plasticity of Adult Stem Cells. Cell *116*, 6*39*–648. https://doi.org/10.1016/s0092-8*67*4(04)00208-9.

3. Kragl, M., Knapp, D., Nacu, E., Khattak, S., Maden, M., Epperlein, H.H., and Tanaka, E.M. (2009). Cells keep a memory of their tissue origin during axolotl limb regeneration. Nature *460*, 60–*65*. https://doi.org/10.1038/nature08*152*.

4. Zawadzka, M., Rivers, L.E., Fancy, S.P.J., Zhao, C., Tripathi, R., Jamen, F., Young, K., Goncharevich, A., Pohl, H., Rizzi, M., et al. (2010). CNS-Resident Glial Progenitor/Stem Cells Produce Schwann Cells as well as Oligodendrocytes during Repair of CNS Demyelination. Cell Stem Cell 6, 578–*59*0. https://doi.org/10.1016/j.stem.2010.04.002.

5. Itoyama, Y., Webster, H.DeF., Richardson, E.P., and Trapp, B.D. (*19*83). Schwann cell remyelination of demyelinated axons in spinal cord multiple sclerosis lesions. Ann. Neurol. *14*, *33*9–346. https://doi.org/10.1002/ana.4101*40313*.

6. Itoyama, Y., Ohnishi, A., Tateishi, J., Kuroiwa, Y., and Webster, H.F. de (1985). Spinal cord multiple sclerosis lesions in Japanese patients: Schwann cell remyelination occurs in areas that lack glial fibrillary acidic protein (GFAP). Acta Neuropathol. 65, *217–22*3. https://doi.org/10.1007/bf006*87*001.

7. Guest, J.D., Hiester, E.D., and Bunge, R.P. (2005). Demyelination and Schwann cell responses adjacent to injury epicenter cavities following chronic human spinal cord injury. Exp. Neurol. *192*, 384–393. https://doi.org/10.1016/j.expneurol.2004.11.033.

8. Wang, Z.H., Walter, G.F., and Gerhard, L. (1996). The expression of nerve growth factor receptor on Schwann cells and the effect of these cells on the regeneration of axons in traumatically injured human spinal cord. Acta Neuropathol. *91*, *18*0–184. https://doi.org/10.1007/s004010050411.

9. Blakemore, W.F. (1976). Invasion of Schwann Cells into the Spinal Cord of a Rat Following Local Injections of Lysolecithin. Neuropathol. Appl. Neurobiol. 2, 21–39. https://doi.org/10.1111/j.*136*5-2990.1976.tb00559.x.

10. Blakemore, W.F. (1982). Ethidium bromide induced demyelination in the spinal cord of the cat. Neuropathol. Appl. Neurobiol. 8, 365–375. https://doi.org/10.1111/j.1365-2990.1982.tb00*30*5.x.

11. Pender, M.P. (1989). Recovery from acute experimental allergic encephalomyelitis in the Lewis rat: early restoration of nerve conduction and repair by Schwann cells and oligodendrocytes. Brain *112*, 393–416. https://doi.org/10.*109*3/brain/112.2.393.

12. Woodruff, R.H., and Franklin, R.J.M. (1999). Demyelination and remyelination of the caudal cerebellar peduncle of adult rats following stereotaxic injections of lysolecithin, ethidium bromide, and complement/anti-galactocerebroside: A comparative study. Glia *25*, 216–228. https://doi.org/10.1002/(sici)1098-1136(19990201)25:3<216::aid-glia2>3.0.co;2-l.

13. Hall, B.K. (2000). The neural crest as a fourth germ layer and vertebrates as quadroblastic not

triploblastic. Evol. Dev. 2, 3–5. https://doi.org/10.1046/j.1525-142x.2000.00032.x.
14. Talbott, J.F., Cao, Q., Enzmann, G.U., Benton, R.L., Achim, V., Cheng, X.X., Mills, M.D., Rao, M.S., and Whittemore, S.R. (2006). Schwann cell-like differentiation by adult oligodendrocyte precursor cells following engraftment into the demyelinated spinal cord is BMP-dependent. Glia *54*, 147–159. https://doi.org/10.1002/glia.20369.
15. Castro, G.M. de, Deja, N.A., Ma, D., Zhao, C., and Franklin, R.J.M. (2015). Astrocyte Activation via Stat3 Signalling Determines the Balance of Oligodendrocyte versus Schwann Cell Remyelination. Am. J. Pathol. *185*, *243*1–2440. https://doi.org/10.1016/j.ajpath.2015.05.011.
16. Ulanska-Poutanen, J., Mieczkowski, J., Zhao, C., Konarzewska, K., Kaza, B., Pohl, H.B., Bugajski, L., Kaminska, B., Franklin, R.J., and Zawadzka, M. (2018). Injury-induced perivascular niche supports alternative differentiation of adult rodent CNS progenitor cells. eLife 7, e30325. https://doi.org/10.7554/elife.30325.
17. Bartus, K., Burnside, E.R., Galino, J., James, N.D., Bennett, D.L.H., and Bradbury, E.J. (2019). ErbB receptor signalling directly controls oligodendrocyte progenitor cell transformation and spontaneous remyelination after spinal cord injury. Glia 67, 1036–1046. https://doi.org/10.1002/glia.23586.
18. Mi, R., Tammia, M., Shinn, D., Li, Y., Martin, R., Mao, H., and Höke, A. (2019). Oligodendrocyte precursors gain Schwann cell-like phenotype and remyelinate axons upon engraftment into peripheral nerves. J. Tissue Eng. Regen. Med. 13, 1854–1860. https://doi.org/10.1002/term.2935.
19. Gautier, H.O.B., Evans, K.A., Volbracht, K., James, R., Sitnikov, S., Lundgaard, I., James, F., Lao-Peregrin, C., Reynolds, R., Franklin, R.J.M., et al. (2015). Neuronal activity regulates remyelination via glutamate signalling to oligodendrocyte progenitors. Nat. Commun. 6, 8*51*8. https://doi.org/10.1038/ncomms9518.
20. Wolf, F.A., Hamey, F.K., Plass, M., Solana, J., Dahlin, J.S., Göttgens, B., Rajewsky, N., Simon, L., and Theis, F.J. (2019). PAGA: graph abstraction reconciles clustering with trajectory inference through a topology preserving map of single cells. Genome Biol. 20, 59. https://doi.org/10.1186/s13059-019-1663-x.
21. Weiler, P., Lange, M., Klein, M., Pe'er, D., and Theis, F. (2024). CellRank 2: unified fate mapping in multiview single-cell data. Nat. Methods 21, 1196–1205. https://doi.org/10.1038/s41592-024-02303-9.
22. Talbott, J.F., Cao, Q., Enzmann, G.U., Benton, R.L., Achim, V., Cheng, X.X., Mills, M.D., Rao, M.S., and Whittemore, S.R. (2006). Schwann cell-like differentiation by adult oligodendrocyte precursor cells following engraftment into the demyelinated spinal cord is BMP-dependent. Glia 54, 147–159. https://doi.org/10.1002/glia.20369.
23. Mabie, P.C., Mehler, M.F., Marmur, R., Papavasiliou, A., Song, Q., and Kessler, J.A. (1997). Bone Morphogenetic Proteins Induce Astroglial Differentiation of Oligodendroglial–Astroglial Progenitor Cells. J. Neurosci. 17, 4112–4120. https://doi.org/10.1523/jneurosci.17-11-04112.1997.
24. Zhao, C., Fancy, S.P.J., Franklin, R.J.M., and ffrench-Constant, C. (2009). Up-regulation of oligodendrocyte precursor cell αV integrin and its extracellular ligands during central nervous system remyelination. J. Neurosci. Res. 87, 3447–3455. https://doi.org/10.1002/jnr.22231.
25. Milner, R., Edwards, G., Streuli, C., and ffrench-Constant, C. (1996). A Role in Migration for the αvβ1 Integrin Expressed on Oligodendrocyte Precursors. J. Neurosci. 16, 7240–7252. https://doi.org/10.1523/jneurosci.16-22-07240.1996.
26. Milner, R., Crocker, S.J., Hung, S., Wang, X., Frausto, R.F., and Zoppo, G.J. del (2007). Fibronectin- and

vitronectin-induced microglial activation and matrix metalloproteinase-9 expression is mediated by integrins alpha5beta1 and alphavbeta5. J. Immunol. (Baltim., Md : 1950) *178*, 8158–8*167*. https://doi.org/10.4049/jimmunol.178.12.8158.
27. Gudz, T.I., Schneider, T.E., Haas, T.A., and Macklin, W.B. (2002). Myelin Proteolipid Protein Forms a Complex with Integrins and May Participate in Integrin Receptor Signalling in Oligodendrocytes. J. Neurosci. 22, 7398–7407. https://doi.org/10.1523/jneurosci.22-17-07398.2002.
28. Sawala, A., Scarcia, M., Sutcliffe, C., Wilcockson, S.G., and Ashe, H.L. (2015). Peak BMP Responses in the Drosophila Embryo Are Dependent on the Activation of Integrin Signalling. Cell Rep. 13, 1519–1520. https://doi.org/10.1016/j.celrep.2015.10.079.
29. Czopka, T., Holst, A. von, ffrench-Constant, C., and Faissner, A. (2010). Regulatory Mechanisms that Mediate Tenascin C-Dependent Inhibition of Oligodendrocyte Precursor Differentiation. J. Neurosci. 30, 12310–12322. https://doi.org/10.1523/jneurosci.4957-09.2010.
30. Zhao, C., Fancy, S.P.J., ffrench-Constant, C., and Franklin, R.J.M. (2008). Osteopontin is extensively expressed by macrophages following CNS demyelination but has a redundant role in remyelination. Neurobiol. Dis. 31, 209–217. https://doi.org/10.1016/j.nbd.2008.04.007.
31. Govier-Cole, A.E., Wood, R.J., Fletcher, J.L., Gonsalvez, D.G., Merlo, D., Cate, H.S., Murray, S.S., and Xiao, J. (2019). Inhibiting Bone Morphogenetic Protein 4 Type I Receptor Signalling Promotes Remyelination by Potentiating Oligodendrocyte Differentiation. eNeuro 6, ENEURO.0399-18.2019. https://doi.org/10.1523/eneuro.0399-18.2019.
32. Felding-Habermann, B., and Cheresh, D.A. (1993). Vitronectin and its receptors. Curr. Opin. Cell Biol. 5, 864–868. https://doi.org/10.1016/0955-0674(93)90036-p.
33. Stoffels, J.M.J., Jonge, J.C. de, Stancic, M., Nomden, A., Strien, M.E. van, Ma, D., Šišková, Z., Maier, O., ffrench-Constant, C., Franklin, R.J.M., et al. (2013). Fibronectin aggregation in multiple sclerosis lesions impairs remyelination. Brain 136, 116–*131*. https://doi.org/10.1093/brain/aws313.
34. Grinspan, J.B., Edell, E., Carpio, D.F., Beesley, J.S., Lavy, L., Pleasure, D., and Golden, J.A. (2000). Stage-specific effects of bone morphogenetic proteins on the oligodendrocyte lineage. J. Neurobiol. 43, 1–17. https://doi.org/10.1002/(sici)1097-4695(200004)43:1<1::aid-neu1>3.0.co;2-0.
35. Baas, D., Bourbeau, D., Sarliéve, L.L., Ittel, M., Dussault, J.H., and Puymirat, J. (1997). Oligodendrocyte maturation and progenitor cell proliferation are independently regulated by thyroid hormone. Glia 19, 324–332. https://doi.org/10.1002/(sici)1098-1136(199704)19:4<324::aid-glia5>3.0.co;2-x.
36. Manno, G.L., Soldatov, R., Zeisel, A., Braun, E., Hochgerner, H., Petukhov, V., Lidschreiber, K., Kastriti, M.E., Lönnerberg, P., Furlan, A., et al. (2018). RNA velocity of single cells. Nature *560*, 494–498. https://doi.org/10.1038/s41586-018-0414-6.
37. Arthur-Farraj, P., Wanek, K., Hantke, J., Davis, C.M., Jayakar, A., Parkinson, D.B., Mirsky, R., and Jessen, K.R. (2011). Mouse schwann cells need both NRG1 and cyclic AMP to myelinate. Glia 59, 720–733. https://doi.org/10.1002/glia.21144.
38. Sim, F.J., Zhao, C., Li, W.-W., Lakatos, A., and Franklin, R.J.M. (2002). Expression of the POU-Domain Transcription Factors SCIP/Oct-6 and Brn-2 Is Associated with Schwann Cell but Not Oligodendrocyte Remyelination of the CNS. Mol. Cell. Neurosci. 20, 669–682. https://doi.org/10.1006/mcne.2002.1145.
39. Küspert, M., Hammer, A., Bösl, M.R., and Wegner, M. (2011). Olig2 regulates Sox10 expression in oligodendrocyte precursors through an evolutionary conserved distal enhancer. Nucleic Acids Res. 39,

1280–1293. https://doi.org/10.1093/nar/gkq951.
40. Liu, Z., Hu, X., Cai, J., Liu, B., Peng, X., Wegner, M., and Qiu, M. (2007). Induction of oligodendrocyte differentiation by Olig2 and Sox10: Evidence for reciprocal interactions and dosage-dependent mechanisms. Dev. Biol. *302*, 683–693. https://doi.org/10.1016/j.ydbio.2006.10.007.
41. Finzsch, M., Schreiner, S., Kichko, T., Reeh, P., Tamm, E.R., Bösl, M.R., Meijer, D., and Wegner, M. (2010). Sox10 is required for Schwann cell identity and progression beyond the immature Schwann cell stage. J. Cell Biol. *189*, 701–712. https://doi.org/10.1083/jcb.200912142.
42. Lu, Q.R., Sun, T., Zhu, Z., Ma, N., Garcia, M., Stiles, C.D., and Rowitch, D.H. (2002). Common Developmental Requirement for Olig Function Indicates a Motor Neuron/Oligodendrocyte Connection. Cell 109, 75–86. https://doi.org/10.1016/s0092-8674(02)00678-5.
43. Zhou, Q., Choi, G., and Anderson, D.J. (2001). The bHLH Transcription Factor Olig2 Promotes Oligodendrocyte Differentiation in Collaboration with Nkx2.2. Neuron 31, 791–807. https://doi.org/10.1016/s0896-6273(01)00414-7.
44. Liu, Z., Jin, Y.-Q., Chen, L., Wang, Y., Yang, X., Cheng, J., Wu, W., Qi, Z., and Shen, Z. (2015). Specific Marker Expression and Cell State of Schwann Cells during Culture In Vitro. PLoS ONE 10, e0123278. https://doi.org/10.1371/journal.pone.0123278.
45. Pol, S.U., Lang, J.K., O'Bara, M.A., Cimato, T.R., McCallion, A.S., and Sim, F.J. (2013). Sox10-MCS5 enhancer dynamically tracks human oligodendrocyte progenitor fate. Exp Neurol *247*, 694–702. https://doi.org/10.1016/j.expneurol.2013.03.010.
46. Shcherbo, D., Murphy, C.S., Ermakova, G.V., Solovieva, E.A., Chepurnykh, T.V., Shcheglov, A.S., Verkhusha, V.V., Pletnev, V.Z., Hazelwood, K.L., Roche, P.M., et al. (2009). Far-red fluorescent tags for protein imaging in living tissues. Biochem. J. *418*, 567–574. https://doi.org/10.1042/bj20081949.
47. Jeffery, N.D., and Blakemore, W.F. (1995). Remyelination of mouse spinal cord axons demyelinated by local injection of lysolecithin. J. Neurocytol. 24, 775–781. https://doi.org/10.1007/bf01191213.
48. Blakemore, W.F., Eames, R.A., Smith, K.J., and Mcdonald, W.I. (1977). Remyelination in the spinal cord of the cat following intraspinal injections of lysolecithin. J. Neurol. Sci. 33, 31–43. https://doi.org/10.1016/0022-510x(77)90179-4.
49. Franklin, R.J.M., and Blakemore, W.F. (1993). Requirements for schwann cell migration within cns environments: A viewpoint. Int. J. Dev. Neurosci. 11, 641–649. https://doi.org/10.1016/0736-5748(93)90052-f.
50. Blakemore, W.F. (1992). Transplanted cultured type-1 astrocytes can be used to reconstitute the glia limitans of the CNS: the structure which prevents Schwann cells from myelinating CNS axons. Neuropathol. Appl. Neurobiol. 18, 460–466. https://doi.org/10.1111/j.1365-2990.1992.tb00812.x.
51. Lerma-Martin, C., Badia-i-Mompel, P., Flores, R.O.R., Sekol, P., Schäfer, P.S.L., Riedl, C.J., Hofmann, A., Thäwel, T., Wünnemann, F., Ibarra-Arellano, M.A., et al. (2024). Cell type mapping reveals tissue niches and interactions in subcortical multiple sclerosis lesions. Nat. Neurosci. 27, 2354–2365. https://doi.org/10.1038/s41593-024-01796-z.
52. Conde, C.D., Xu, C., Jarvis, L., Rainbow, D., Wells, S., Gomes, T., Howlett, S., Suchanek, O., Polanski, K., King, H., et al. (2022). Cross-tissue immune cell analysis reveals tissue-specific features in humans. Sci. (N. York, NY) *376*, eabl5197–eabl5197. https://doi.org/10.1126/science.abl5197.
53. Troulé, K., Petryszak, R., Cakir, B., Cranley, J., Harasty, A., Prete, M., Tuong, Z.K., Teichmann, S.A.,

Garcia-Alonso, L., and Vento-Tormo, R. (2025). CellPhoneDB v5: inferring cell–cell communication from single-cell multiomics data. Nat. Protoc., 1–29. https://doi.org/10.1038/s41596-024-01137-1.
54. Yan, K.S., Chia, L.A., Li, X., Ootani, A., Su, J., Lee, J.Y., Su, N., Luo, Y., Heilshorn, S.C., Amieva, M.R., et al. (2012). The intestinal stem cell markers Bmi1 and Lgr5 identify two functionally distinct populations. Proc. Natl. Acad. Sci. 109, 466–471. https://doi.org/10.1073/pnas.1118857109.
55. Tian, H., Biehs, B., Warming, S., Leong, K.G., Rangell, L., Klein, O.D., and Sauvage, F.J. de (2011). A reserve stem cell population in small intestine renders Lgr5-positive cells dispensable. Nature *478*, 255–259. https://doi.org/10.1038/nature10408.
56. Thorel, F., Népote, V., Avril, I., Kohno, K., Desgraz, R., Chera, S., and Herrera, P.L. (2010). Conversion of adult pancreatic α-cells to β-cells after extreme β-cell loss. Nature *464*, 1149–1154. https://doi.org/10.1038/nature08894.
57. Jessen, K.R., Mirsky, R., and Arthur-Farraj, P. (2015). The Role of Cell Plasticity in Tissue Repair: Adaptive Cellular Reprogramming. Dev. Cell 34, 613–620. https://doi.org/10.1016/j.devcel.2015.09.005.
58. Jessen, K.R., Mirsky, R., and Lloyd, A.C. (2015). Schwann Cells: Development and Role in Nerve Repair. Cold Spring Harb. Perspect. Biol. 7, a020487. https://doi.org/10.1101/cshperspect.a020487.
59. Castro, G.M. de, Deja, N.A., Ma, D., Zhao, C., and Franklin, R.J.M. (2015). Astrocyte Activation via Stat3 Signalling Determines the Balance of Oligodendrocyte versus Schwann Cell Remyelination. Am. J. Pathol. 185, 2431–2440. https://doi.org/10.1016/j.ajpath.2015.05.011.
60. Harburger, D.S., and Calderwood, D.A. (2009). Integrin signalling at a glance. J. Cell Sci. *122*, 1472–1472. https://doi.org/10.1242/jcs.052910.
61. Colognato, H., Ramachandrappa, S., Olsen, I.M., and ffrench-Constant, C. (2004). Integrins direct Src family kinases to regulate distinct phases of oligodendrocyte development. J. Cell Biol. 167, 365–375. https://doi.org/10.1083/jcb.200404076.
62. Yu, Y., Chen, Y., Kim, B., Wang, H., Zhao, C., He, X., Liu, L., Liu, W., Wu, L.M.N., Mao, M., et al. (2013). Olig2 Targets Chromatin Remodelers to Enhancers to Initiate Oligodendrocyte Differentiation. Cell 152, 248–261. https://doi.org/10.1016/j.cell.2012.12.006.
63. Samanta, J., and Kessler, J.A. (2004). Interactions between ID and OLIG proteins mediate the inhibitory effects of BMP4 on oligodendroglial differentiation. Development 131, 4131–4142. https://doi.org/10.1242/dev.01273.
64. Wilusz, J.E., JnBaptiste, C.K., Lu, L.Y., Kuhn, C.-D., Joshua-Tor, L., and Sharp, P.A. (2012). A triple helix stabilizes the 3′ ends of long noncoding RNAs that lack poly(A) tails. Genes Dev. 26, 2392–2407. https://doi.org/10.1101/gad.204438.112.
65. Kim, Y.J., Lim, H., Li, Z., Oh, Y., Kovlyagina, I., Choi, I.Y., Dong, X., and Lee, G. (2014). Generation of Multipotent Induced Neural Crest by Direct Reprogramming of Human Postnatal Fibroblasts with a Single Transcription Factor. Cell Stem Cell 15, 497–506. https://doi.org/10.1016/j.stem.2014.07.013.
66. Duncan, G.J., Manesh, S.B., Hilton, B.J., Assinck, P., Liu, J., Moulson, A., Plemel, J.R., and Tetzlaff, W. (2018). Locomotor recovery following contusive spinal cord injury does not require oligodendrocyte remyelination. Nat. Commun. 9, 3066. https://doi.org/10.1038/s41467-018-05473-1.
67. GrandPré, T., Nakamura, F., Vartanian, T., and Strittmatter, S.M. (2000). Identification of the Nogo inhibitor of axon regeneration as a Reticulon protein. Nature 403, 439–444. https://doi.org/10.1038/35000226.

68. Mukhopadhyay, G., Doherty, P., Walsh, F.S., Crocker, P.R., and Filbin, M.T. (1994). A novel role for myelin-associated glycoprotein as an inhibitor of axonal regeneration. Neuron 13, 757–767. https://doi.org/10.1016/0896-6273(94)90042-6.
69. Jessen, K.R., and Mirsky, R. (2016). The repair Schwann cell and its function in regenerating nerves. J. Physiol. *594*, 3521–3531. https://doi.org/10.1113/jp270874.
70. Sofroniew, M.V. (2020). Astrocyte Reactivity: Subtypes, States, and Functions in CNS Innate Immunity. Trends Immunol. 41, 758–770. https://doi.org/10.1016/j.it.2020.07.004.
71. Hamby, M.E., and Sofroniew, M.V. (2010). Reactive Astrocytes As Therapeutic Targets for CNS Disorders. Neurotherapeutics 7, 494–506. https://doi.org/10.1016/j.nurt.2010.07.003.
72. Chen, C.Z., Neumann, B., Förster, S., and Franklin, R.J.M. (2021). Schwann cell remyelination of the central nervous system: why does it happen and what are the benefits? Open Biol. 11, 200352. https://doi.org/10.1098/rsob.200352.
73. Gao, Y., and Zhao, Y. (2014). Self-processing of ribozyme-flanked RNAs into guide RNAs in vitro and in vivo for CRISPR-mediated genome editing. J. Integr. Plant Biol. 56, 343–349. https://doi.org/10.1111/jipb.12152.
74. Challis, R.C., Kumar, S.R., Chan, K.Y., Challis, C., Beadle, K., Jang, M.J., Kim, H.M., Rajendran, P.S., Tompkins, J.D., Shivkumar, K., et al. (2019). Systemic AAV vectors for widespread and targeted gene delivery in rodents. Nat. Protoc. 14, 379–414. https://doi.org/10.1038/s41596-018-0097-3.
75. Sim, F.J., Zhao, C., Penderis, J., and Franklin, R.J.M. (2002). The Age-Related Decrease in CNS Remyelination Efficiency Is Attributable to an Impairment of Both Oligodendrocyte Progenitor Recruitment and Differentiation. J. Neurosci. 22, 2451–2459. https://doi.org/10.1523/jneurosci.22-07-02451.2002.
76. Livak, K.J., and Schmittgen, T.D. (2001). Analysis of Relative Gene Expression Data Using Real-Time Quantitative PCR and the 2−ΔΔCT Method. Methods 25, 402–408. https://doi.org/10.1006/meth.2001.1262.
77. Picelli, S., Faridani, O.R., Björklund, Å.K., Winberg, G., Sagasser, S., and Sandberg, R. (2014). Full-length RNA-seq from single cells using Smart-seq2. Nat. Protoc. 9, 171–181. https://doi.org/10.1038/nprot.2014.006.
78. Yu, Y., Chen, C.Z., Celardo, I., Tan, B.W.Z., Hurcomb, J.D., Leal, N.S., Popovic, R., Loh, S.H.Y., and Martins, L.M. (2024). Enhancing mitochondrial one-carbon metabolism is neuroprotective in Alzheimer's disease models. Cell Death Dis. 15, 856. https://doi.org/10.1038/s41419-024-07179-3.
79. Heumos, L., Schaar, A.C., Lance, C., Litinetskaya, A., Drost, F., Zappia, L., Lücken, M.D., Strobl, D.C., Henao, J., Curion, F., et al. (2023). Best practices for single-cell analysis across modalities. Nat. Rev. Genet. 24, 550–572. https://doi.org/10.1038/s41576-023-00586-w.
80. Keenan, A.B., Torre, D., Lachmann, A., Leong, A.K., Wojciechowicz, M.L., Utti, V., Jagodnik, K.M., Kropiwnicki, E., Wang, Z., and Ma'ayan, A. (2019). ChEA3: transcription factor enrichment analysis by orthogonal omics integration. Nucleic Acids Res. 47, W212–W224. https://doi.org/10.1093/nar/gkz446.
81. Szklarczyk, D., Kirsch, R., Koutrouli, M., Nastou, K., Mehryary, F., Hachilif, R., Gable, A.L., Fang, T., Doncheva, N.T., Pyysalo, S., et al. (2022). The STRING database in 2023: protein–protein association networks and functional enrichment analyses for any sequenced genome of interest. Nucleic Acids Res. 51, D638–D646. https://doi.org/10.1093/nar/gkac1000.

82. Lopez, R., Regier, J., Cole, M.B., Jordan, M.I., and Yosef, N. (2018). Deep generative modeling for single-cell transcriptomics. Nat. Methods 15, 1053–1058. https://doi.org/10.1038/s41592-018-0229-2.
83. Xu, C., Prete, M., Webb, S., Jardine, L., Stewart, B.J., Hoo, R., He, P., Meyer, K., and Teichmann, S.A. (2023). Automatic cell type harmonization and integration across Human Cell Atlas datasets. bioRxiv, 2023.05.01.538994. https://doi.org/10.1101/2023.05.01.538994.
84. Troulé, K., Petryszak, R., Prete, M., Cranley, J., Harasty, A., Tuong, Z.K., Teichmann, S.A., Garcia-Alonso, L., and Vento-Tormo, R. (2023). CellPhoneDB v5: inferring cell-cell communication from single-cell multiomics data. arXiv. https://doi.org/10.48550/arxiv.2311.04567.

FIGURES

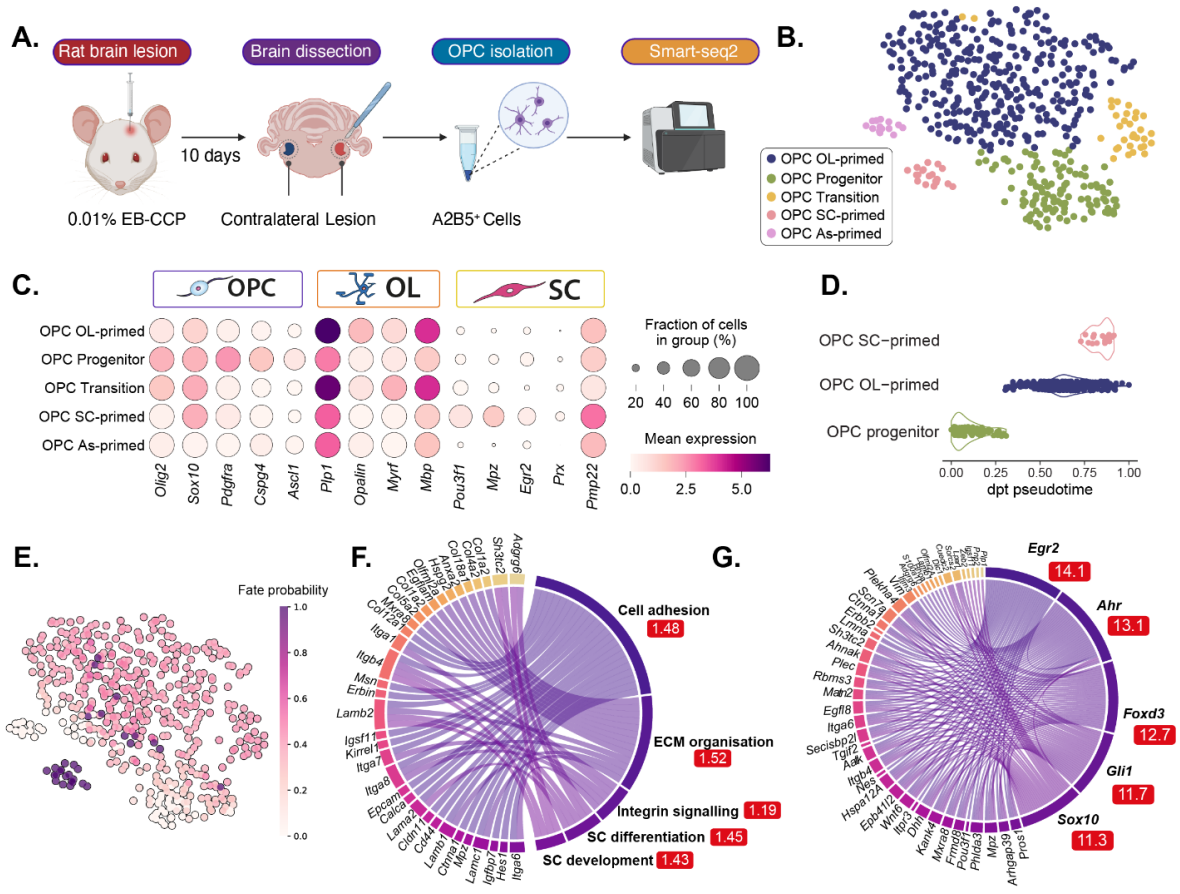

Figure 1: Single-cell transcriptomic analysis of purified A2B5+ OPCs.

A. Purification of A2B5⁺ OPCs purification for single-cell RNA profiling via Smart-seq2. OPCs from the lesioned caudal cerebellar peduncle (CCP) and the uninjured contralateral side were collected and submitted for sequencing. A total of six animals were used: three animals underwent unilateral lesioning, from which both the lesioned and uninjured contralateral sides were sequenced, and three unlesioned animals served as naïve controls.

B. Unsupervised clustering of single-cell transcriptional profiles from 517 A2B5⁺ cells. Five different states of OPCs were identified using Leiden clustering. Based on marker genes (shown in Figure 1C and Supplementary Figure 1E). these clusters were annotated as oligodendrocyte-primed (OL-primed, in dark blue), OPC progenitor in green, SC-primed (coral), transitioning cells (yellow), and astrocyte-primed (pink).

C. Expression of lineage-enriched genes across different clusters used for classification of the cell states. An extended list is shown in Supplementary Figure 1E.

D. Diffusion pseudotime values across different cell clusters. Each dot represents a cell and the distribution is shown as a violin plot.

E. Fate probabilities of individual cells transitioning toward a SC-like state.

F. Pathway enrichment analysis of the genes significantly associated with the cell fate probabilities shown in Figure 1E. The enrichment scores are shown in the red boxes. The top 200 genes were analysed on

STRING, and only the top 5 pathways are shown. An extended table is available here: https://izu0421.github.io/opc2sc.

G. Transcription factor analysis of the top 200 cell fate drivers. The enrichment scores are shown in the red boxes. Only the top 5 TFs from the GTEx library analysis of ChEA3 are shown. An extended table is available here: https://izu0421.github.io/opc2sc.

Supplementary Figure 1: Transcriptomic analyses confirm data robustness and reveal that SC-primed OPCs are unique to the lesion.

A-B. UMAP visualisation stratified by batch (**A**) and by condition (**B**).

C. Differential abundance analysis based on K-nearest neighbours using Milo. Cells from clusters that are significantly increased (spatial FDR<0.05) in the injury condition are labelled in red. No cell clusters were significantly decreased in this comparison.

D. Expression of a SC gene score, calculated using a list of SC-related genes (*Mpz, Prx, Egr2, Sox10, Pou3f1*) subtracted by the average expression of a random set of reference genes. **E.** Dot plot showing extended marker gene expression across different OPC sub-populations. The analysis includes genes associated with SC identity, myelination, nerve support, and CNS glial cell lineages (OPCs, oligodendrocytes, and

astrocytes). **F**. Trajectory analysis to predict the differentiation pseudotime using graph abstraction. **G.** Expression of a set of fate driver genes identified in Figure 1E using CellRank that are related to the Wnt pathway.

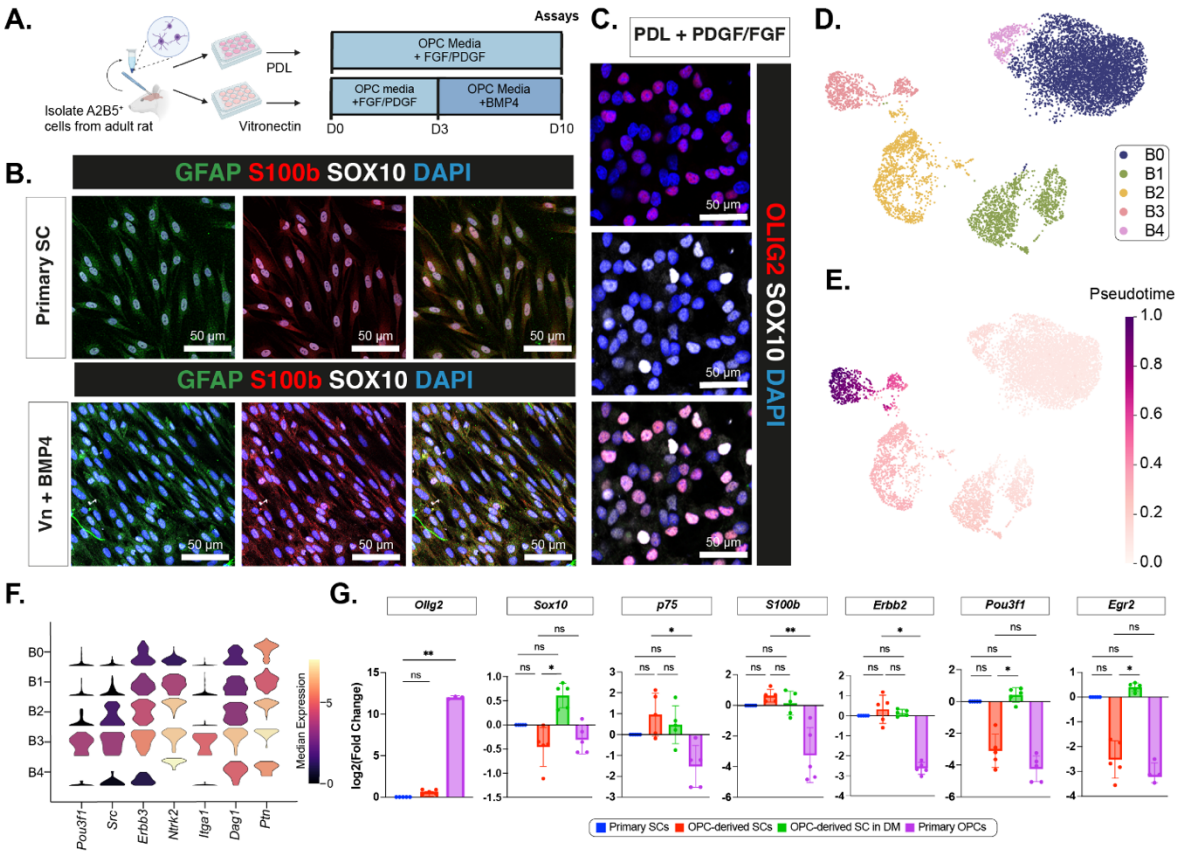

Figure 2: Vitronectin and BMP4 is sufficient to drive OPC to Schwann cell differentiation.

A. A2B5$^+$ were isolated from the whole adult rat brain, then seeded on PDL or vitronectin coated plates. Control OPCs were plated on PDL and maintained in OPC media containing FGF/PDGF. To induce SC differentiation, OPCs were cultured on vitronectin (Vn), allowed to recover in standard OPC media for 3 days, then changed into BMP4-media for a week.

B. GFAP, S100b and SOX10 immunostaining of cultured primary SCs and OPC-derived SCs generated using Vn and BMP4. Data are representative of three independent experiments.

C. OLIG2 and SOX10 immunostaining of OPCs cultured in OPC proliferation medium. Representative of three independent experiments

D. UMAP representation of scRNA-seq data from Vn/BMP4-induced oSCs reveals five distinct cellular clusters.

E. RNA velocity-predicted pseudotime of the Vn/BMP4-induced oSCs.

F. Expression levels of SC genes in oSCs treated with Vn/BMP4, stratified by cluster.

G. RT-qPCR of *Olig2, Sox10, p75, S100b, Erbb2, Pou3f12 and Egr2* expression in primary SCs, OPC-derived SCs, OPC-derived SCs in differentiation medium (DM) (containing cAMP and NRG1) and primary OPCs. Gene expression values are normalised to primary SCs. Values are mean ± SD. (*p< 0.05, **p< 0.01, by Kruskal-Wallis test with Dunn's multiple comparison test; ns, not significant). Five biological replicates were used per group.

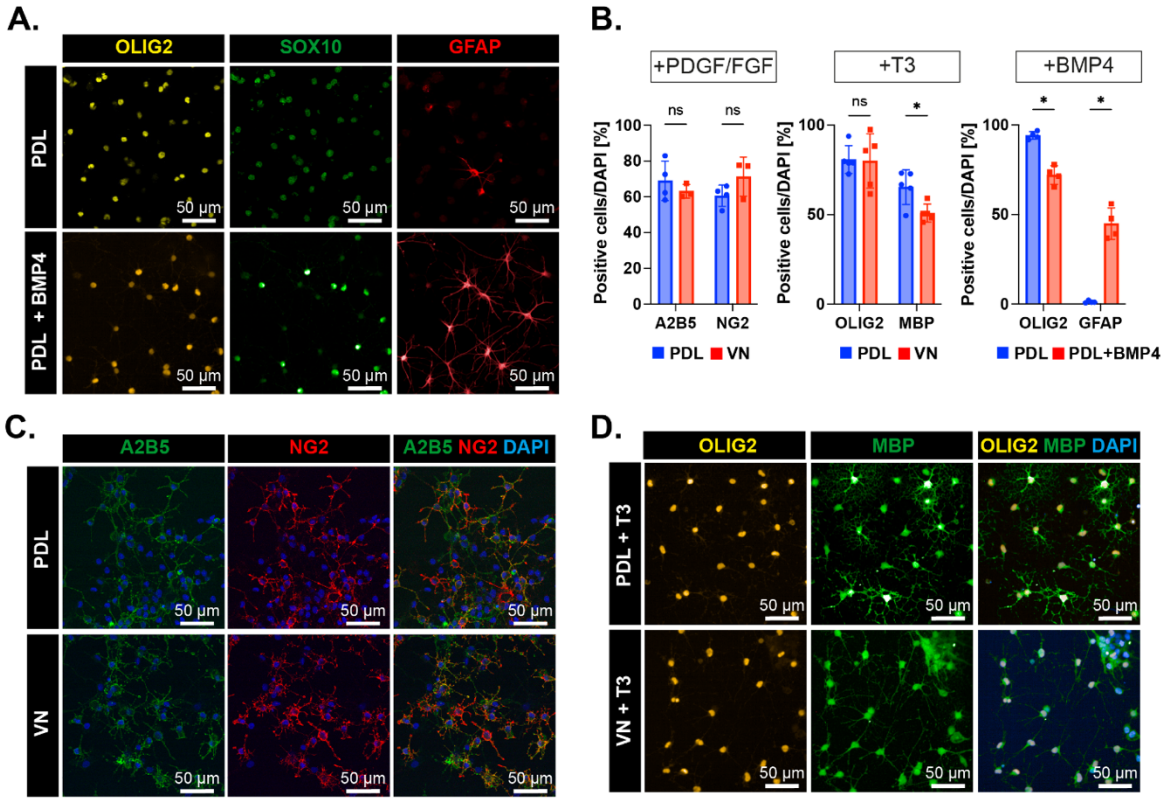

Supplementary Figure 2: Vitronectin or BMP4 alone cannot induce OPC-to-SC differentiation.
A. OLIG2, SOX10, and GFAP immunostaining of OPCs cultured on PDL with an without BMP4.
B. Quantification of cells immunostained for A2B5, NG2, OLIG2, MBP, or GFAP under the specified conditions. Values are mean ± SD, (*p< 0.05, **p< 0.01 by unpaired t-test; ns, not significant). Data from at least three independent experiments.
C. A2B5 and NG2 immunostaining of OPCs cultured on PDL or vitronectin under proliferation conditions.
D. OLIG2 and MBP immunostaining of OPCs cultured on PDL or vitronectin under differentiation conditions.

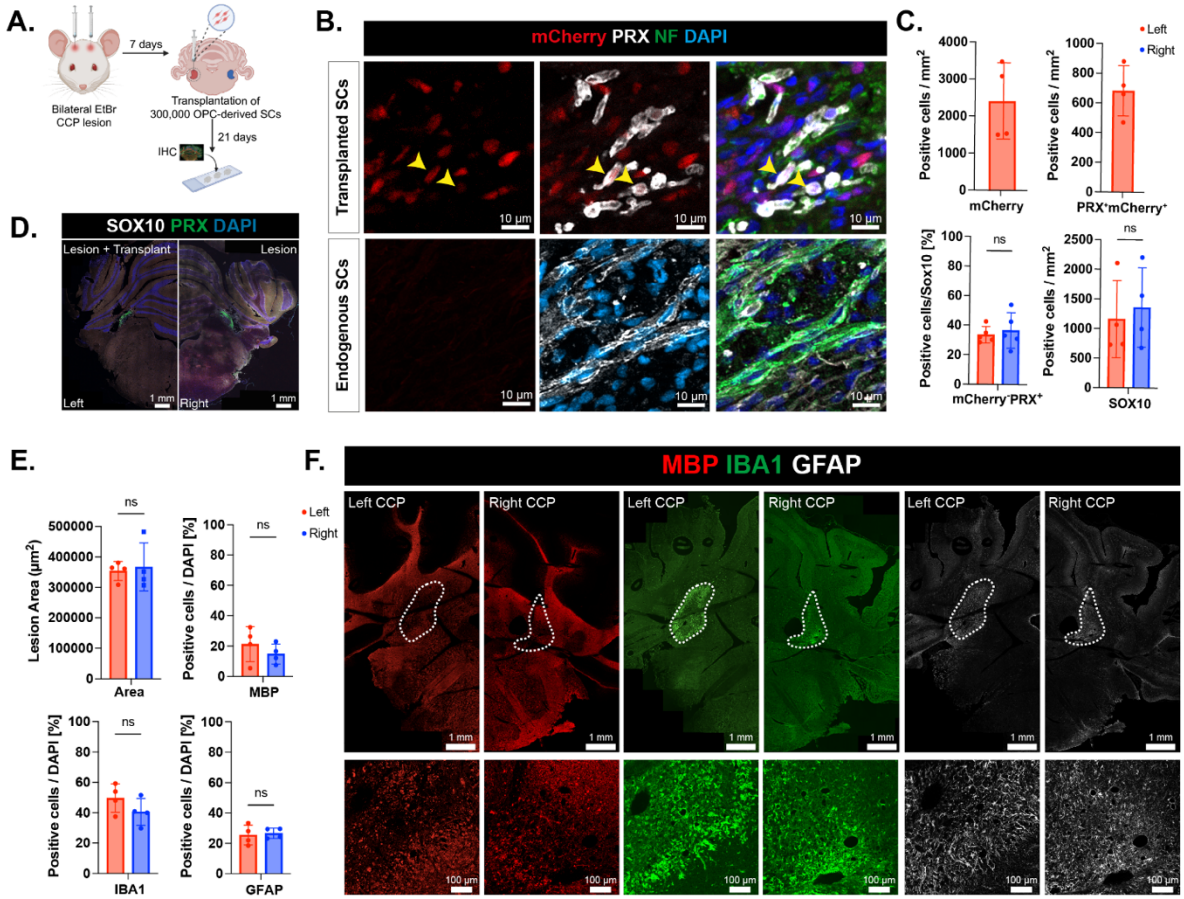

Figure 3: Transplanted oSCs integrate and form peripheral-style myelin in the CNS

A. Schematic overview of the brain lesioning and cell transplantation experiment. Bilateral EtBr brain lesioning was performed, then one week later 300,000 mCherry labelled OPC-derived SCs were transplanted unilaterally into the left CCP. Animals were perfused 21 days after transplantation (28 days post-lesion, dpl) to assess remyelination.

B. Immunohistochemistry of the transplanted area showing mCherry and PRX at 21 days post-transplant (28 dpl). Arrows indicate transplanted cells co-expressing mCherry and PRX. The bottom panel shows endogenous SC remyelination, identified by cells that are $PRX^{+}mCherry^{-}$.

C. Quantification of the number of mCherry, SOX10 and PRX-positive cells within the lesion.

D. Immunohistochemistry of brain lesioning shows SOX10, mCherry, and PRX protein expression

E. Quantification of the lesion area, and the number of MBP, IBA1, and GFAP-positive cells within the lesion.

F. MBP, IBA1, and GFAP immunostaining to visualise the bilateral lesion and unilateral transplant area at 28 dpl

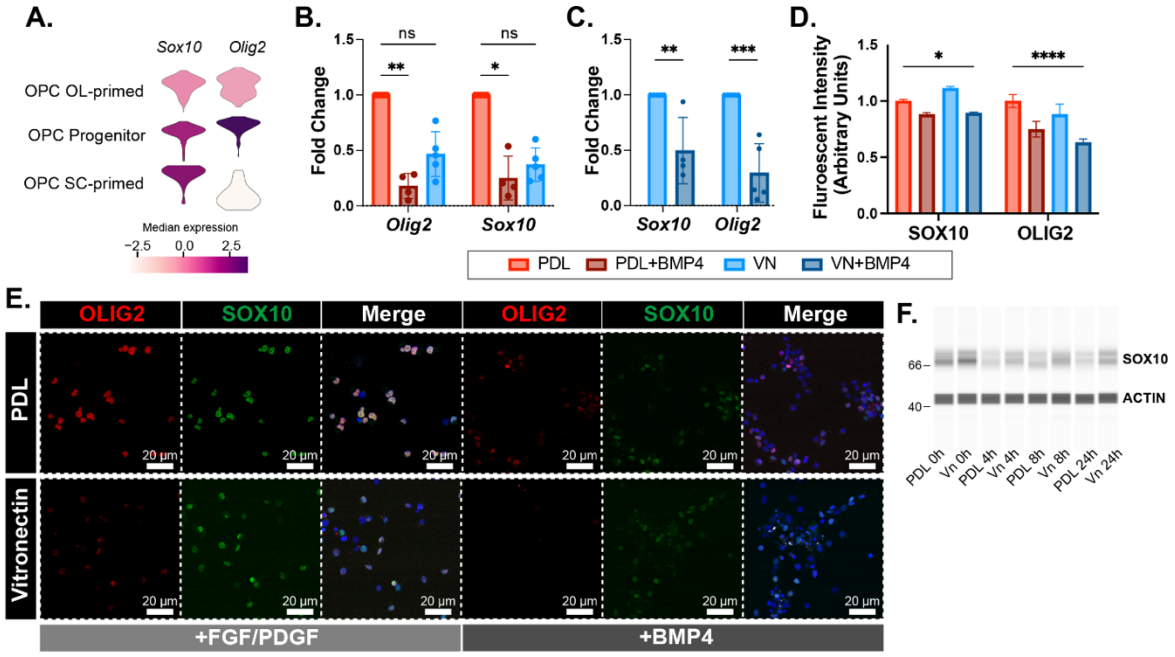

Figure 4: BMP4 decreases OLIG2 and SOX10 levels, but vitronectin stabilises SOX10 protein.

A. Expression levels of *Olig2* and *Sox10* from the Smart-seq dataset, comparing SC-primed OPCs to OPCs remaining within the oligodendroglial lineage.
B. RT-qPCR analysis of *Olig2* and *Sox10* mRNA expression in OPCs cultured on PDL or vitronectin, with or without BMP4 treatment. Values are mean ± SD, normalised to the PDL control condition. Statistical significance was determined by Kruskal-Wallis non-parametric test (*$p < 0.05$, **$p<0.01$), followed by Dunn's post-hoc test.
C. RT-qPCR analysis of *Olig2* and *Sox10* mRNA expression in OPCs cultured on Vn with or without BMP4 treatment. Data are normalised to samples cultured on vitronectin. Statistical significance was determined by Kruskal-Wallis non-parametric test (**$p < 0.01$, ***$p<0.001$), followed by Dunn's post-hoc test. RT-qPCR experiments were conducted with four biological replicates per group.
D. Quantification of fluorescent intensity of SOX10 and OLIG2 in OPCs cultured on PDL or vitronectin under standard proliferation conditions (+PDGF/FGF) or following BMP4 treatment. Values are normalised to cells cultured on PDL. Values are mean ± SD, by two-way ANOVA with Šidák's multiple comparison test.
E. Representative immunohistochemistry images of SOX10 and OLIG2 OPCs cultured on vitronectin or PDL with or without BMP4. Representative data from three independent experiments.
F. OPCs were cultured on PDL or vitronectin (Vn) and treated with cycloheximide. A Jess Simple western blot shows SOX10 and ACTB protein levels at 0, 4, 8, and 24 hours. Experiment representative of three biological replicates.

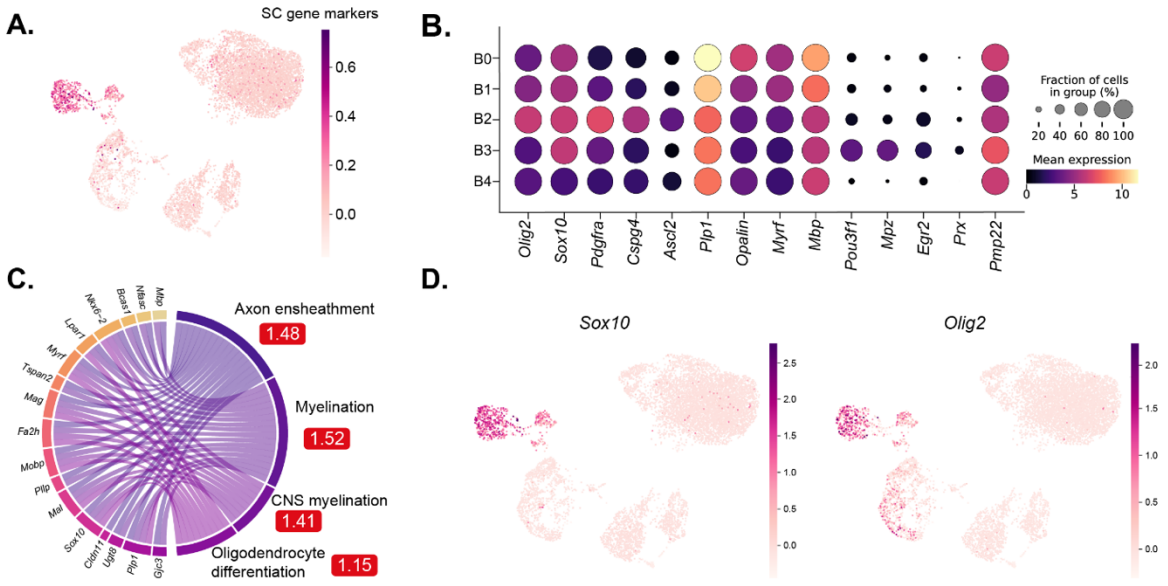

Supplementary Figure 3: Extended characterisation of Vn/BMP4-induced oSCs

A. Expression of SC gene score composed of SC genes including (*Mpz*, *Prx*, *Egr2*, *Sox10* and *Pou3f1*) in oSCs treated with Vn/BMP4.

B. Expression dotplot of key lineage and functional marker genes across the five Vn/BMP4 treated OPC subclusters.

C. Pathway enrichment analysis of the top 200 fate driver genes identified using CellRank2 and their corresponding pathways. The enrichment scores are shown in red boxes. Only a subset of pathways are shown; an extended list is available here: https://izu0421.github.io/opc2sc.

D. Expression of *Sox10* and *Olig2* in Vn/BMP4-induced oSCs.

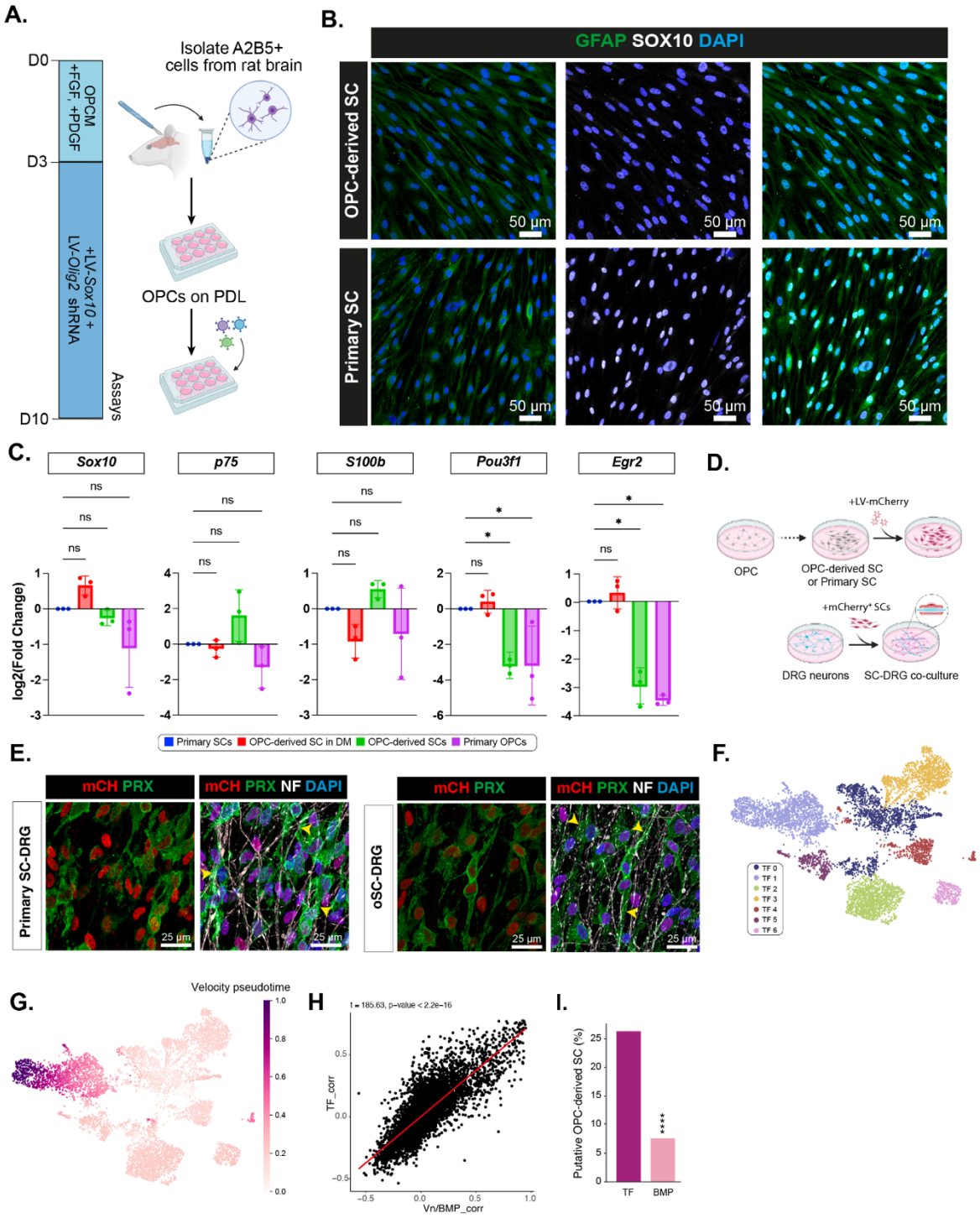

Figure 5: Suppressing Olig2 and stabilising Sox10 activity is sufficient to induce OPCs to convert into Schwann *cells in vitro*.

A. Induction of OPC-to-SC differentiation. OPCs were isolated from an adult rat brain, then maintained in OPC proliferation medium (+FGF, +PDGF) to allow cells to recover for three days. Lentiviruses encoding

Sox10, *rTTA*, and *Olig2* shRNA were then added to infect OPCs, which were subsequently cultured until day 10 (D10).

B. Immunostaining for GFAP and SOX10 in OPC-derived SC and primary SC cultures.

C. RT-qPCR analysis of myelinating SC markers (*Sox10*, *Pou3f1*, and *Egr2*), and immature/non-myelinating SC markers (*p75* and *S100b*) in primary OPCs, OPC-derived SCs, and primary SCs. The bar graph shows mean gene expression ± SD. Gene fold change is normalised to primary SCs. Data are presented as mean ± SD. Statistical significance was determined by Kruskal-Wallis test followed by Dunn's multiple comparisons test; *p< 0.05, **p< 0.01, ***p< 0.001, ****p< 0.0001, ns, not significant). Each group included at least three biological replicates.

D. Schematic showing SC-DRG co-culture experiment. SCs were pre-labeled with LV-mCherry before being seeded onto DRGs to exclude the possibility of SC contaminants in DRG preparations.

E. Immunostaining of PRX and mCherry in myelinating co-cultures of DRGs with either mCherry-labelled OPC-derived SC or primary SCs. Data are representative of at least three independent experiments.

F. UMAP representation of scRNA-seq data from the TF-induced oSCs reveals seven cellular clusters.

G. RNA velocity analysis of TF-induced oSCs.

H. Correlation between SC cell fate driver genes in the TF-induced (y axis) and BMP/Vn-treated (x axis) datasets (Pearson's product-moment correlation, t = 185.63, p-value < 2.2e-16). Each dot represents a gene.

I. Bar graph showing the percentage of oSCs from BMP4/Vn (BMP) and TF-treated OPCs out of the total number that passed quality control and were sequenced.

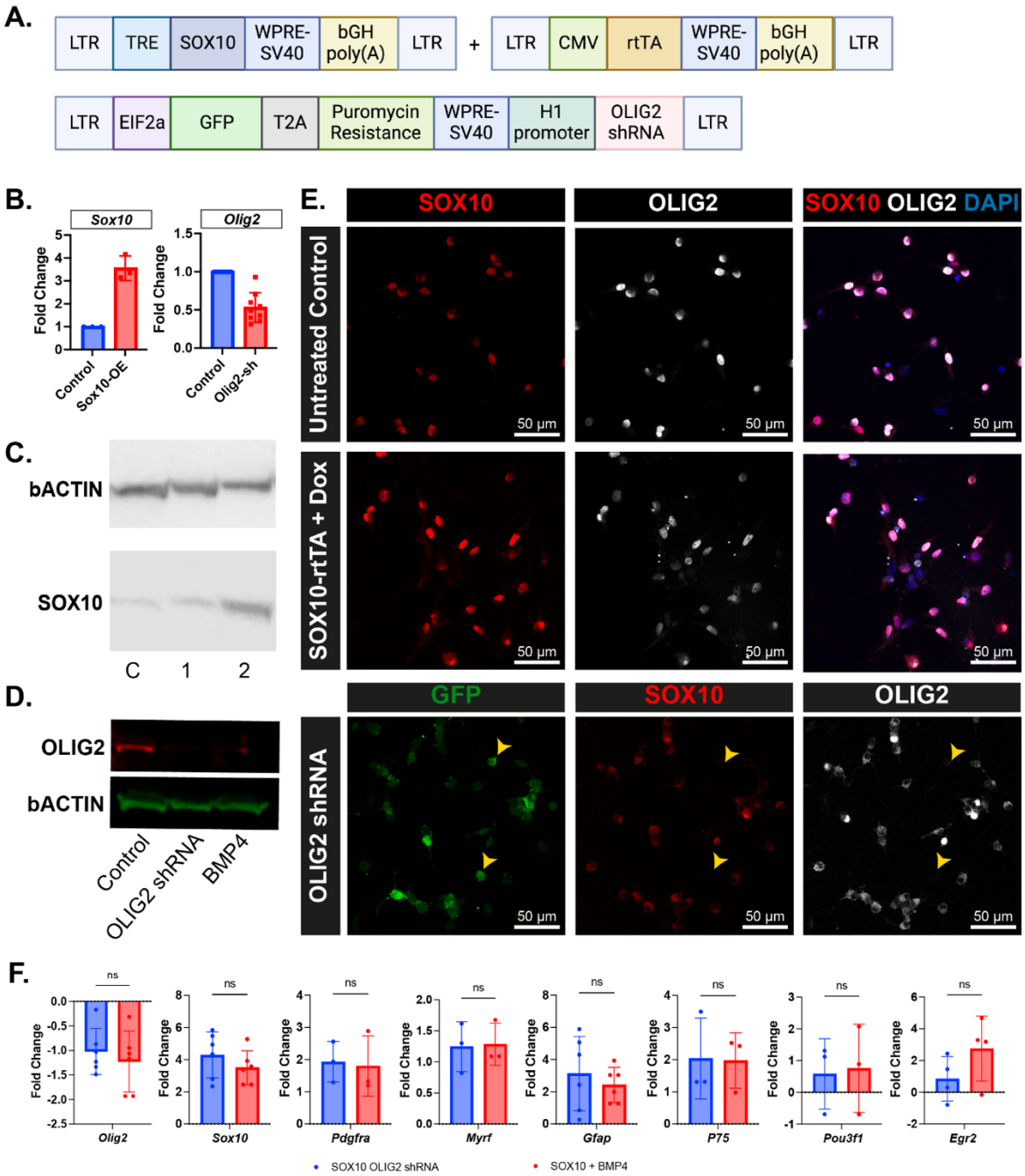

Supplementary Figure 4: Generation and validation of constructs to overexpress Sox10 and to knockout Olig2.

A. Schematic linear map of the LV-Sox10, LV-rtTA and LV-OLIG2shRNA plasmid constructs.

B. RT-qPCR analysis of *Olig2* and *Sox10* mRNA expression in cells infected with LV-Sox10, or LV-Olig2 shRNA, compared to uninfected controls. Values are presented as mean ± SD. (*p< 0.05, **p< 0.01, ***p< 0.001, ****p< 0.0001 by unpaired t-test; ns, not significant).

C. Western blot showing SOX10 protein levels in OPC lysates. Lanes represent: (C) untreated controls, (1) cells infected with LV-TRE-Sox10 only, and (2) cells co-infected with LV-TRE-Sox10 and LV-CMV-rtTA.
D. Western blot showing OLIG2 protein levels in OPCs treated with LV-Olig2shRNA compared to untreated and BMP4-treated controls.
E. SOX10 immunostaining in OPCs infected with LV-TRE-Sox10 and LV-CMV-rtTA compared to untreated controls. The figure also includes images of GFP^+ cells, which were infected with LV-OLIG2 shRNA, showing the fluorescence intensity of SOX10 and OLIG2. Data are representative of three independent experiments.
F. RT-qPCR analysis of oligodendroglial genes (*Olig2*, *Sox10*, *Pdgfra*, *Myrf*) and SC lineage genes (*Gfap*, *p75*, *Oct*, *Krox20*) in OPCs treated with LV-Sox10 and LV-OLIG2shRNA versus LV-Sox10 and BMP4. Values are mean ± SD, (*$p< 0.05$, **$p< 0.01$, ***$p< 0.001$, ****$p< 0.0001$ by unpaired t-test; ns, not significant).

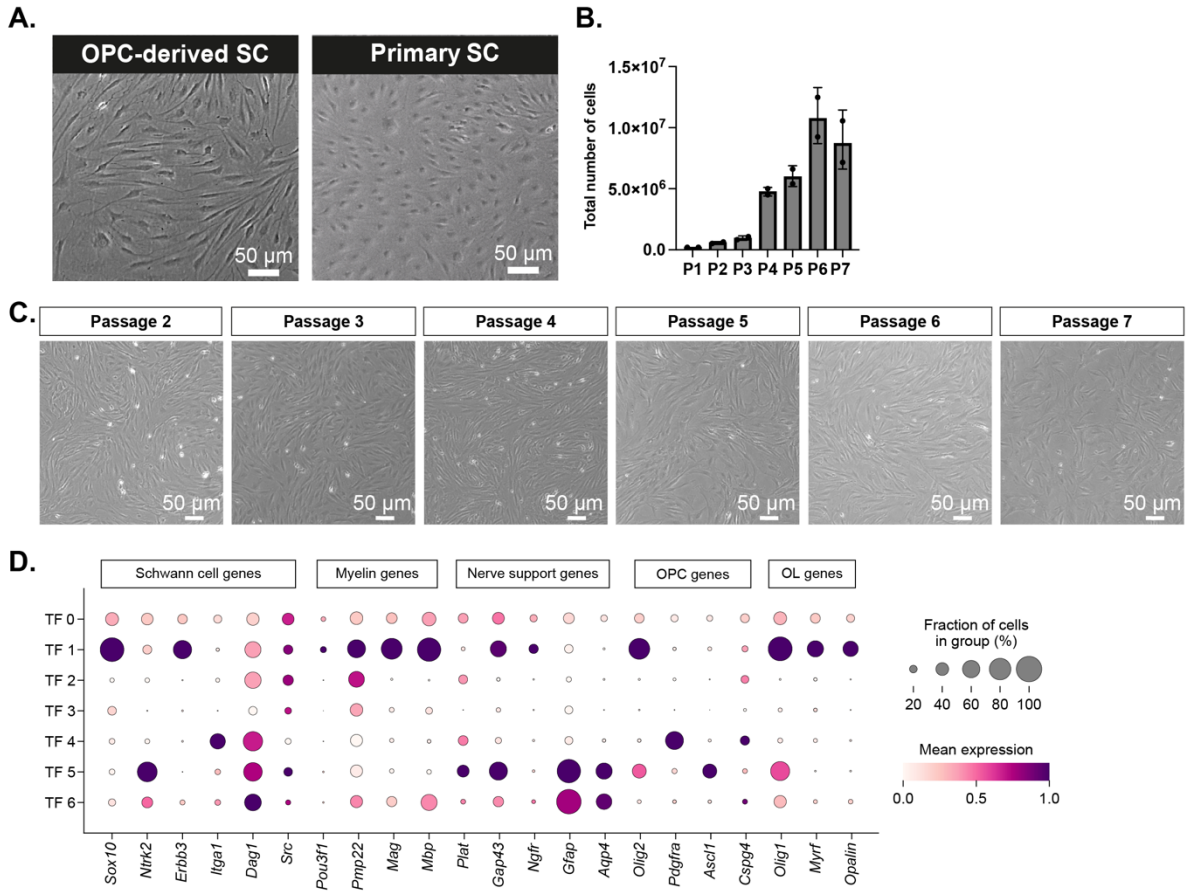

Supplementary Figure 5 - Extended characterization of OPC-derived Schwann cells

A. Bright-field images of oSCs and primary SCs.
B. Total number of TF-induced oSCs from passage 2 (P2) to passage 7 (P7). Values are mean ±SD.
C. Representative bright-field images of oSCs at different passages (P2 to P7).
D. Expression of SC lineage-associated transcription factors and functional markers across the seven cell clusters, shown in Figure 5F.

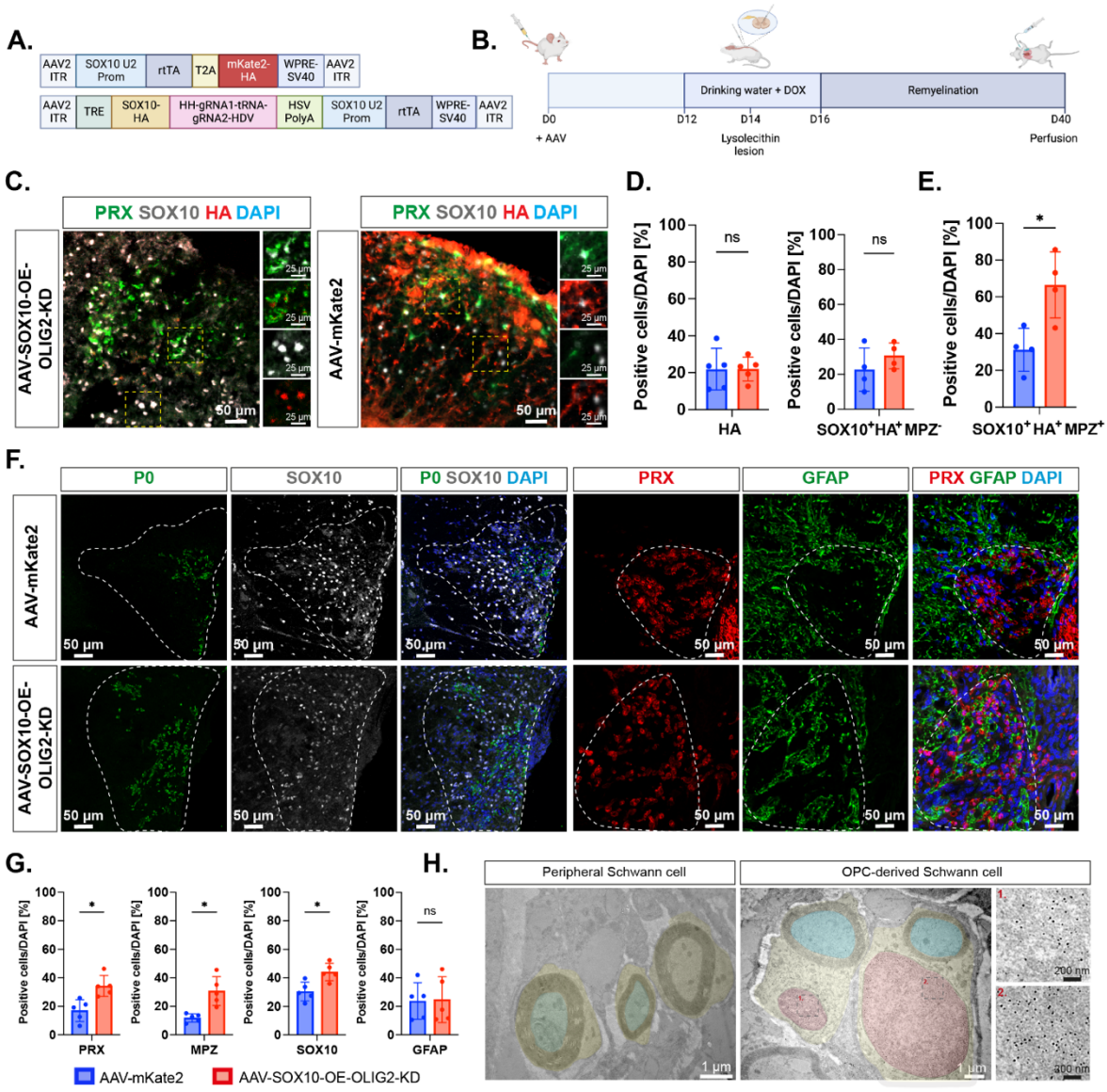

Figure 6 *Olig2* downregulation and *Sox10* overexpression are sufficient to induce OPC differentiation into SCs *in vivo*

A. Schematic linear map of the AAV-SOX10-OLIG2-gRNA and AAV-mKate2 plasmid constructs.

B. Schematic of the experimental overview. Animals received either AAV-SOX10-OLIG2-gRNA or AAV-mKate2 via tail vein injection, followed by doxycycline administration in drinking water from D12 to D16. At D14 post-injection, a focal lysolecithin-induced demyelinating lesion was created in the spinal cord. Remyelination was assessed at D40, three weeks after demyelination.

C. Representative immunohistochemistry images of lesioned spinal cords at 21 dpl showing $SOX10^{+}PRX^{+}HA^{-}$ cells (endogenously arising SCs) and $SOX10^{+}PRX^{+}HA^{+}$ cells (OPC-derived SCs infected by the AAV) in both treatment groups.

D. Quantification of HA+ and $SOX10^{+}MPZ^{+}HA^{-}$ cells in the spinal cord lesion.

E. Quantification of $SOX10^{+}MPZ^{+}HA^{+}$ cells in the spinal cord lesion.

F. Immunohistochemistry of the lesion area PRX, MPZ, and GFAP.

G. Quantification of (E) shows a significant increase in the number of PRX$^+$, MPZ$^+$, and Sox10$^+$ cells in animals treated with AAV-SOX10-OLIG2-gRNA compared to AAV-mKate2-treated animals. Values are presented as mean ± SD. (*$p < 0.05$, ns, not significant, by unpaired t-test). The above data was obtained from four biological replicates per group, with at least three fields of view quantified per replicate.
H. Immuno-electron microscopy image showing the ultrastructure of an HA$^+$ SCs within the spinal cord. The SC body is pseudocoloured yellow, the associated axon in blue and the SC nucleus in red. The inset highlights immunogold particle labelling of HA in the SC nucleus.

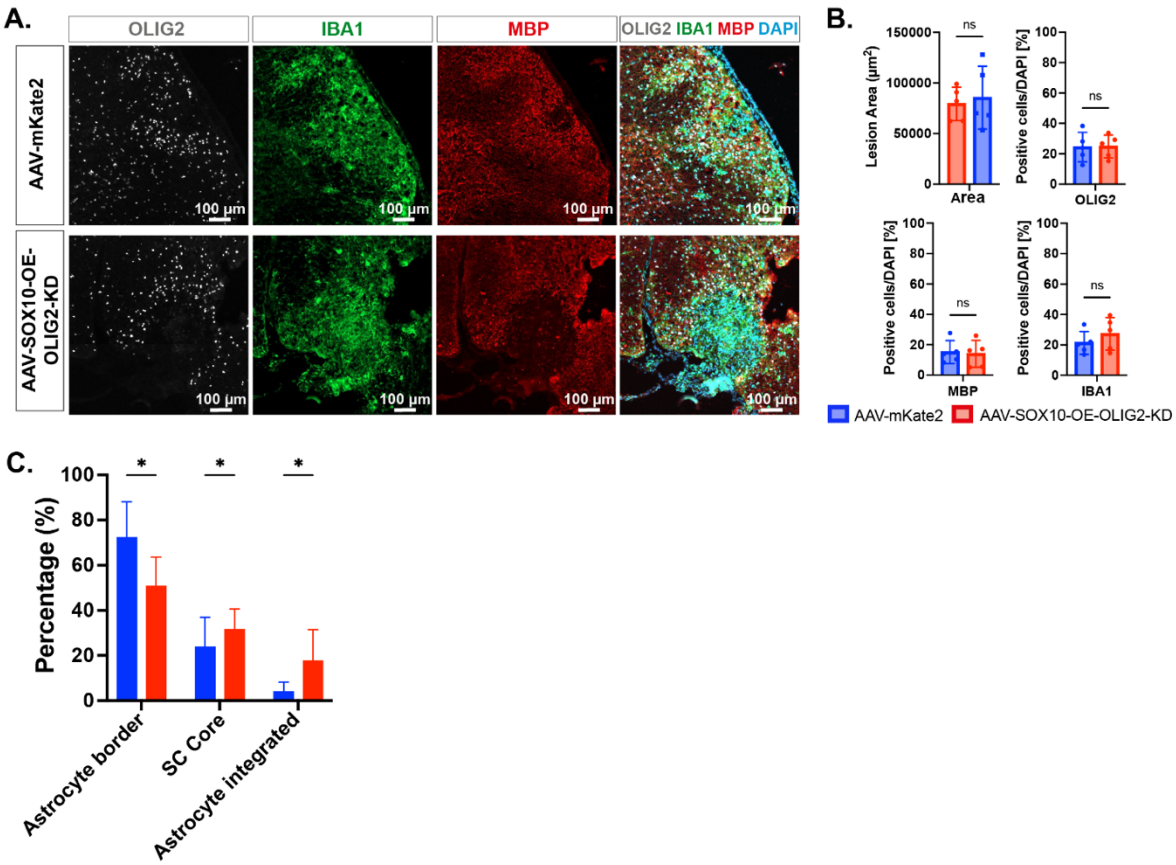

Supplementary Figure 6: AAV induction does not alter lesion dynamics following demyelination

A. Immunostaining of OLIG2, IBA1 and MBP in the lesion area.
B. Quantification of the data presented in **A.** The bar graphs show the lesion size and the number of OLIG2$^+$, MBP$^+$, and IBA1$^+$ cells in animals receiving AAV-SOX10-OLIG2-gRNA or AAV-mKate2-treated animals. Values are expressed as mean ± SD. Statistical significance was determined by one-way ANOVA with Tukey's multiple comparisons test.
C. Quantification of the spatial relationship between PRX$^+$ SCs and GFAP$^+$ astrocytes in the lesion site.

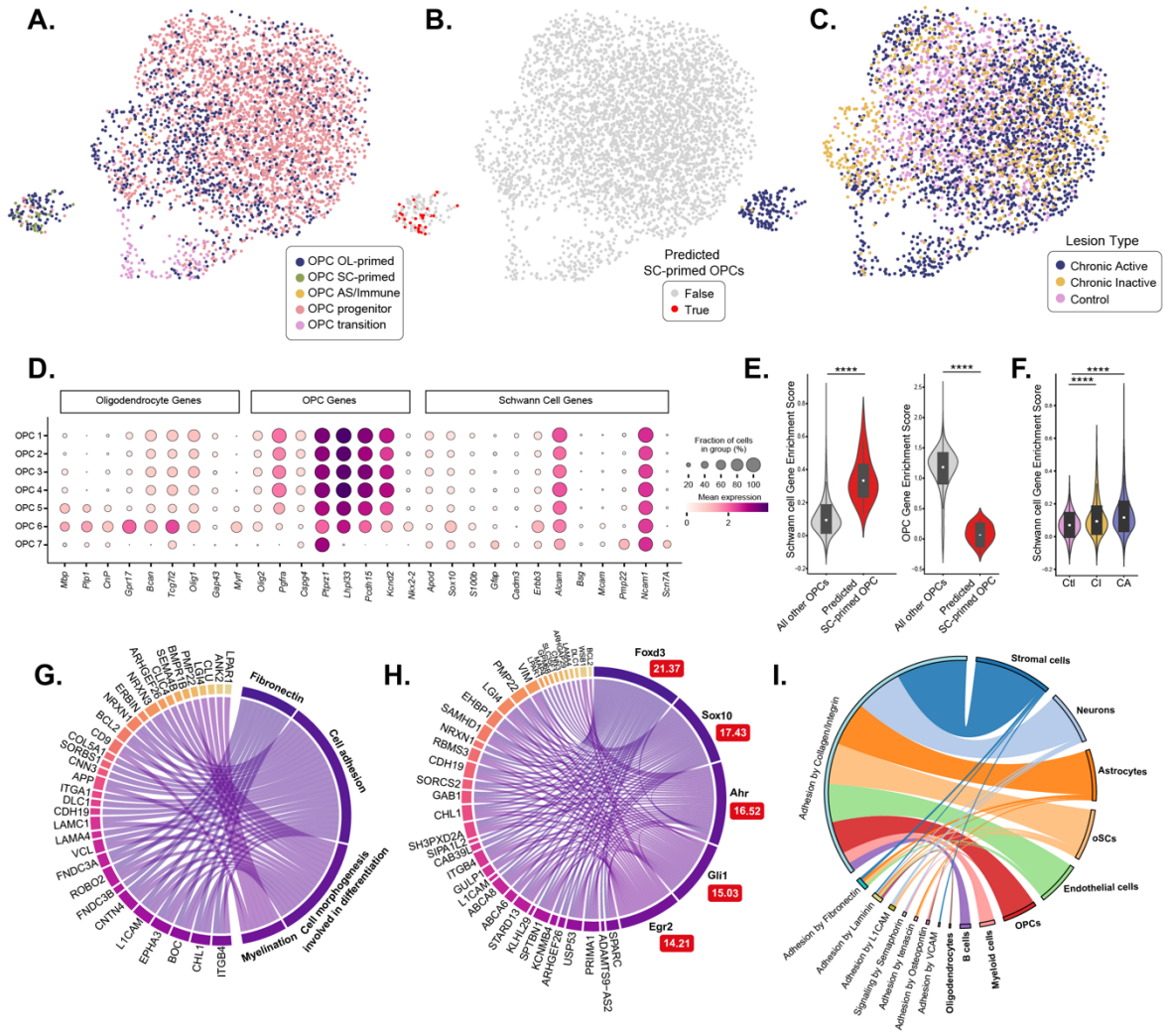

Figure 7: Identification of putative oSCs in OPCs from patients active MS lesions.

A. Human OPC cell states from the Lerma-Martin et al., 2024 dataset were predicted using a CellTypist model trained on scRNA profiling of rat OPCs as described in Figure 1. The human OPCs were mapped onto the embeddings from the rat Smartseq2 dataset to assign cell type identities.

B. UMAP projection highlighting OPCs with a predicted SC-primed identity**,** coloured in red, while all other cells are shown in grey.

C. UMAP projection of OPCs from the Lerma-Martin et al., 2024 dataset, with cells coloured by disease category.

D. Expression of myelin genes, nerve support genes, and SC genes across the 7 Leiden clusters. These clusters were determined from independent clustering of the dataset and is further detailed in Supplementary Figure 7A.

E. Expression of SC genes (left; ****p = 2.058 e-18) or OPC genes (right; ***p = 3.461e-21) in predicted oSCs compared to all other OPCs. Statistical significance was determined by a Mann-Whitney U test.

F. Comparison of SC gene scores from OPCs isolated from control (Ctl), chronic inactive (CI) or chronic active (CA) human brain samples. Statistical significance was determined by a linear mixed effect model.

G. The top 200 differentially expressed genes of the predicted oSCs compared to other OPCs and their associated biological pathways.
H. The top 200 differentially expressed genes of the predicted oSCs compared to other OPCs and the predicted TFs that regulate them. The enrichment scores are shown in the red boxes.
I. L-receptor interactions between oSCs and other cell types in the brain. The class of interaction by adhesion is on the left, and cell types on the right are highlighted in bold.

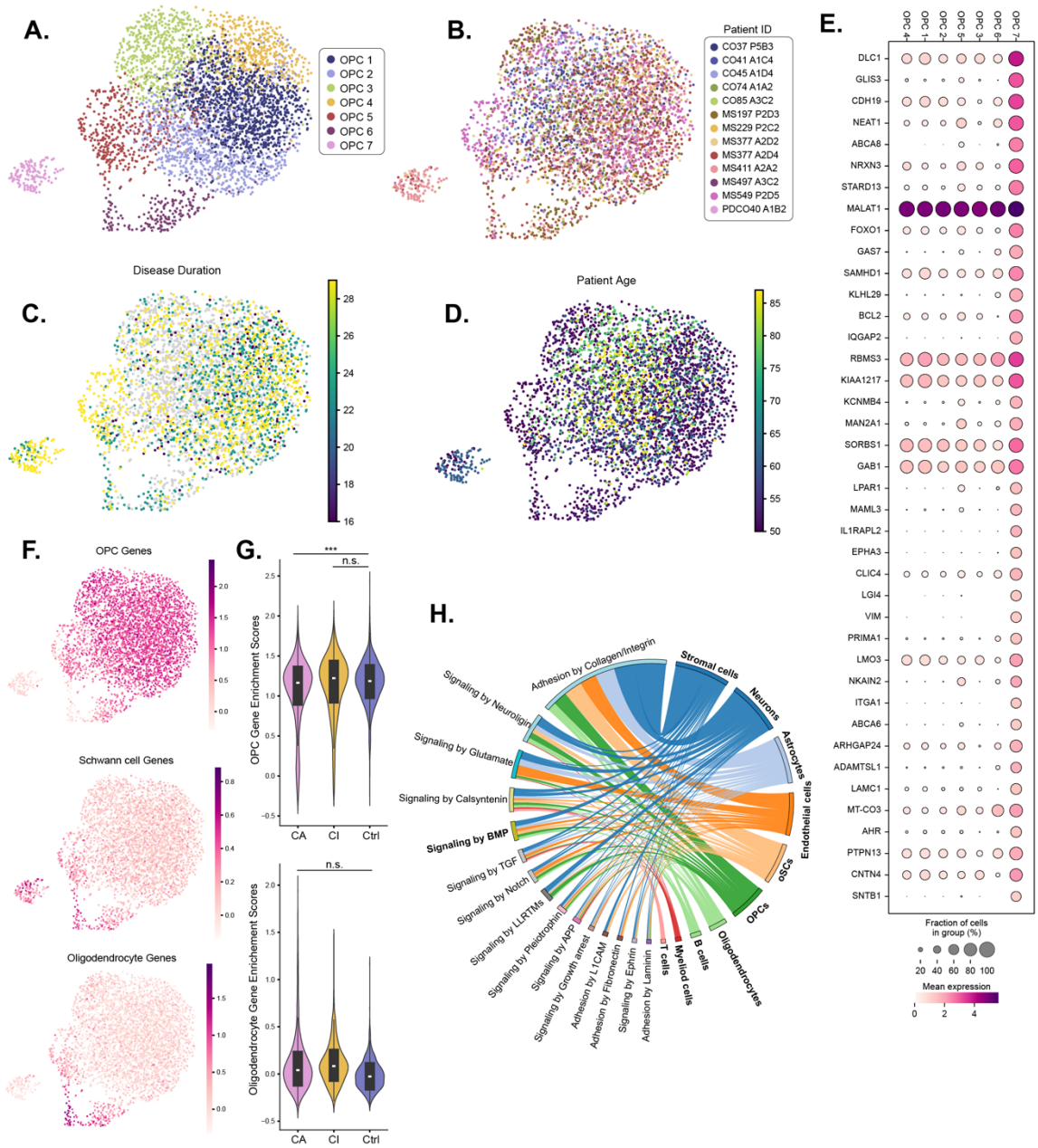

Supplementary Figure 7: Extended characterisation of SC-primed OPCs in human MS

A-D. UMAP projection of OPCs from the Lerma-Martin et al., 2024 dataset with cells coloured by **A.** Leiden clusters, **B.** patient ID, **C.** disease duration (in years, grey dots correspond to nuclei where that data was not available) and **D**. patient age.

E. Top differentially expressed genes from the predicted SC-primed OPCs (Cluster 7) across the seven OPC subclusters. Significance was determined using the Wilcoxon rank sum test with FDR adjustment.

F. UMAP projections of OPCs, with cells coloured by their enrichment scores for lineage gene signatures of OPCs (Top), SCs (Middle) and OLs (Bottom). The list of marker genes used to calculate the enrichment scores is described in Table S3.

G. Violin plots showing the scores of OPC and oligodendrocyte gene signatures, stratified by disease condition: chronic inactive (CI), chronic active (CA), and control.
H. Ligand-receptor interactions between oSCs and other cell types in the brain. The class of signalling pathways is on the left, and cell types on the right are highlighted in bold.

SUPPLEMENTARY TABLES

Table S1: List of antibodies used in this study

Antibody Name	Catalogue Number	Company	Host	Dilution
A2B5	MAB312	Millipore	Mouse	1:1000
bACTIN	AB6276	Abcam	Mouse	1:500
B-III-Tubulin	MMS-435P	Biolegend	Mouse	1:1000
CC1	MABC200	Sigma	Mouse	1:500
GFAP	AB46744	Abcam	Chicken	1:2000
HA	26183	Invitrogen	Mouse	1:500
IBA1	AF5076	Abcam	Goat	1:500
MAP2	AB5392	Abcam	Mouse	1:1000
MBP	MCA4095	Serotec	Rat	1:200
mCherry	AB125096	Abcam	Mouse	1:500
NG2	AB5320	Sigma-Aldrich	Rabbit	1:500
OLIG2	AB9610	Abcam	Rabbit	1:500
OLIG2	MABN50	Sigma-Aldrich	Mouse	1:500
MPZ	AB134439	Abcam	Chicken	1:500
PRX	HPA001868	Cambridge Bioscience	Rabbit	1:500
SM132	801701	Biolegend	Mouse	1:1000
SOX10	AF2864	R&D	Goat	1:200
SOX10	AB155279	R&D	Rabbit	1:500

Table S2: List and sequence of qPCR primers used in this study

Gene	Forward	Reverse
Erbb2	TGACAAGCGCTGTCTGCCG	CTTGTAGTGGGCGCAGGCTG
Gapdh	ACCCAGAAGACTGTGGATGG	CACATTGGGGGTAGGAACAC
Gfap	AGTGGTATCGGTCCAAGTTTGC	TGGCGGCGATAGTCATTAGC
Krox20	GGAGGCCCCTTTGATCAGAT	TGGTTTCTAGGCGCAGAGAT
Mbp	GTCGTAGGCCCCCTTGAATC	GCCTGTCCCTCAGCAGATTT
Myrf	TCTTCGAAGGCCACGACATC	TCAGGGAAGVAGAGGTCAG
Pou3f1	CCTCCTGGCCTTAACGAACG	GTAGGGAAACAGGCGGAAGG
p75	ACCGACAACCTCATTCCTGT	TTGTTTGCAGCTGTTCCACC
Pdgfra	GCCTCCATTCTGGAGCTTGT	CTCGATGTTCGGAAGAGGG
S100b	CAGGGAGAGAGGGTGACAAG	TCCAGCGTCTCCATCACTTT
Sox10	TGCTGCTATCCAGGCTCACTA	TCCCTTTTGGGATCTGCCTTG
TBP	CATCATGAGAATAAGAGAGCC	GGATTGTTCTTCACTCTTGG
Olig2	Quantitect Primer Assay	QT00386505

Table S3: List of genes used to calculate OPC, SC and Oligodendrocyte enrichment scores

OPC Markers	Schwann cell markers	Oligodendrocyte markers
Olig2	Sox10	Mbp
Pdgfra	S100b	Mog
Cspg4	Mbp	Cnpase
Ptprz	Mpz	Gpr17
Enpp6	Mag	Bcan
Lhfpl3	Plp1	Tcf7i2
Pcdh15	P75ntr	Olig1
Kcnd2	Glut1	Olig2
Nkx2.2	Gfap	Gpc5
Olig1	Necl1	Gap43
Apod	Cd44	Myrf
	Cd49e	Plp1
	Cd98	Cldn11
	Erbb3	Opalin
	Slitrk6	
	Cd166	
	Cd147	
	Cd146	
	Pmp22	
	Ncam1	
	L1cam	
	Scn7a	
	Nes	
	Ngfr	
	Top2a	
	Pou3f1	
	Egr2	
	Dhh	